5-2023

An isostable coordinate based amelioration strategy to mitigate the effects of Jet lag

Talha Ahmed
University of Tennessee, Knoxville, tahmed4@vols.utk.edu

To the Graduate Council:

I am submitting herewith a thesis written by Talha Ahmed entitled "An isostable coordinate based amelioration strategy to mitigate the effects of Jet lag." I have examined the final electronic copy of this thesis for form and content and recommend that it be accepted in partial fulfillment of the requirements for the degree of Master of Science, with a major in Electrical Engineering.

Dan D. Wilson, Major Professor

We have read this thesis and recommend its acceptance:

Seddik M. Djouadi, Amir Sadovnik

Accepted for the Council:
Dixie L. Thompson

Vice Provost and Dean of the Graduate School

(Original signatures are on file with official student records.)

An isostable coordinate based amelioration strategy to mitigate the effects of Jet lag

A Thesis Presented for the

Master of Science

Degree

The University of Tennessee, Knoxville

Talha Ahmed

May 2023

Acknowledgments

First and foremost, the credit goes to my academic supervisor, Dr. Dan Wilson, without whom I would not have been able to complete this thesis. I still remember the countless meetings I had with him where he selflessly guided me to ensure that I was on the right track and made consistent progress in my work. Along with being the lead PI for this work, he was also part of my defense committee. I also want to sincerely thank Dr. Seddik Djouadi and Dr. Amir Sadovnik for being part of my defense committee as well. Last but not least, this could not have been done without the constant love and support of my parents.

This material is based upon work supported by the National Science Foundation (NSF) under Grant No. CMMI-1933583.

Abstract

Commercial air travel has become extremely commonplace in the last 20 to 30 years especially as the world has moved towards new heights of globalization. Though air travel has greatly reduced transit times allowing people to cover thousand of miles within hours, it comes with its fair share of issues. jet-lag can be regarded to be at the top of those list of problems; jet-lag typically results from rapid travel through multiple time zones which causes a significant misalignment between the person's internal circadian clock and the external time. A person's circadian clock is governed by a population of coupled neurons entrained to a 24-hour light and dark cycle and thus after rapid air travel, the neuron population needs a certain time to get accustomed to the new time zone. This misalignment can result in a variety of health problems including, but not limited to, lethargy, insomnia and adverse effects to the sleep cycle.

Various techniques have been proposed and are currently in use for jet-lag treatment like melatonin ingestion or making drastic changes to one's own routine prior to air travel. However, these treatment strategies are normally accompanied with long re-entrainment times or following a strict schedule to help with correcting the sleep cycle. The presented work explores an alternate strategy for jet-lag treatment using the notion of operational phase and isostable coordinates for model reduction and then, applying optimal control to derive inputs which can be applied directly to the model. To show the framework's efficacy, results are presented by applying the strategy to a 2-d model; preliminary results show that the proposed approach greatly reduces the reentrainment time required to acclimatize to the new time zone.

Disclosure Statement

The content presented in this thesis is based upon the work done in [1] authored by myself and my supervisor, Dr. Dan Wilson and published in **Chaos: An Interdisciplinary Journal of Nonlinear Science**. Equal amount of work was done by both authors in the formulation of the problem, devising the methodology and the illustrations presented in the publication. Some figures and large chunks of text have been taken from the published paper and reproduced from [1], with the permission of AIP publishing for the purpose of this thesis; some results and strategies discussed in the paper are not included in the thesis. Necessary additions and omissions were made to all the chapters included in the thesis document and the content was paraphrased where necessary.

Table of Contents

List of Figures

Chapter 1

Introduction

Before the 20th century, travel by road and by sea were the conventional ways of travel used by the common masses to travel around the world; this involved long journey times typically around a few days to months depending upon the destination. It was not until commercial flights became popular and relatively inexpensive in the 20th century that these long travel times just got reduced to hours. This not only brought a much needed ease in travel but also exponentially enhanced connectivity and drastically saved time; a person living in UK can now hop on a flight and land in US for a business meeting within a span of a few hours where as the same journey by sea can take weeks on end. However, air travel was accompanied with its own set of problems mainly jet-lag.

Jet-lag generally results when multiple time zones are covered consecutively during air travel; this results in a mismatch between one's own internal circadian clock and the associated environmental time [3], [53]. This internal circadian clock is governed by a set of roughly 20,000 coupled neurons located in the suprachiasmatic nucleus (SCN) [50], [44]; these neurons comprise the master circadian pacemaker within the mammalian brain and their collective oscillation yields a robust endogenous circadian cycle with a near 24-hour period. Normally, these circadian rhythms are entrained to daily time cues such as a 24-hour light-dark cycle [22], [77]; such circadian rhythms are evolutionarily advantageous, allowing for the anticipation of and subsequent response to daily environmental changes [45], [79]. However, as depicted in Fig 1.1, circadian misalignment can arise during air travel resulting in jet-lag accompanied with many health problems. Primarily a sleep disorder, the primary

symptoms of jet-lag are insomnia, daytime fatigue, and a general feeling of malaise [24], [53]. However, additional accumulating evidence suggests that chronic jet-lag could be associated with long term cognitive deficits and accelerated tumor growth [20], [12], [14], [33], [21], [60].

To decrease the reentrainment time following rapid travel across multiple time zones, recent years have seen a surge in interest pertaining to development of jet-lag mitigation strategies. For instance, modeling studies have identified optimal schedules for rapidly acclimating to a new time zone through light avoidance and exposure [4], [80], [17], [55]; some of these strategies have been implemented successfully in real-time using smartphone apps and features [6]. However, all these aforementioned strategies generally require people to strictly follow the prescribed routines for days in advance requiring non-trivial effort. From a dynamical systems perspective, various works in literature often employ phase-based model reduction as an initial approach in order to simplify the circadian models and ultimately, derive applicable jet-lag mitigation strategies.

Phase-only model reduction techniques of the form (2.2) are often employed to study behaviors such as entrainment, circadian misalignment, and jet-lag recovery [72], [25], [59], [37], [47], [71], [81]. PRCs that capture the response to light and melatonin have been measured experimentally in humans [41], [30], [10], [38]. Based on this information, practical jet-lag recovery treatments have been developed such as carefully timed combinations of light exposure and light avoidance [11], [63], evening ingestion of melatonin after eastward travel [46], [58], [5], and combinations of both [51]. Other strategies for jet-lag prevention have been suggested which seek to shift one's circadian rhythm pre-flight [52], [16], [9] as would be useful when peak-level performance is necessary immediately in the new time zone (e.g., for professional athletes [54]).

It is to be noted that a significant limitation of these phase-only reduced models is that they require the oscillator's state to remain close to the nominal limit cycle $x^\gamma(t)$. As such, these models neglect important information about the amplitude dynamics, often referred to as adaptation or memory, that characterizes how the system adapts in response to large magnitude inputs. It is well-established that measured phase response curves to light depend on the history of light stimulation [48], [61], [27], [56], [15] and preliminary evidence suggests that related memory-based effects could have a profound impact on jet-lag recovery. For

instance, the authors of [2] found that desynchronizing the phases of neurons within the SCN greatly reduced the time required to recover from subsequent time shifts in the light schedule. Additionally, [78] showed that blocking vasopressin signaling in mouse SCN allowed for faster recovery to subsequent shifts in a 24-hour light-dark cycle.

Therefore, the primary purpose of the work presented in this thesis is to investigate the influence of circadian memory (i.e., the notion that past inputs have a lingering effect on the dynamics) in the context of recovery from circadian misalignment. In order to capture memory effects that are neglected by the standard phase reduction (2.1), the proposed framework employs an operational phase and isostable coordinate based approach suggested by [69] in which phase is defined with respect to a distinct feature of a given limit cycle. Unlike reduction techniques that use an asymptotic definition of phase, to leading order, the operational phase dynamics depend on the amplitude coordinates allowing us to consider circadian memory. Furthermore, using a calculus of variation framework, an optimal control based jet-lag pretreatment strategy is explored that exploits circadian memory to prime one's circadian cycle to recover quickly in response to an anticipated time-zone shift. This strategy is fundamentally different than those suggested in [52], [16], [9] (which exchange circadian misalignment in one's destination time zone for misalignment in one's home time zone).

The layout of the thesis is as follows: Chapter 2 gives a detailed theoretical background of the techniques and the coordinate transformations used for model reduction in the work along with a detailed literature review on other jet-lag treatment strategies. Meanwhile, Chapter 3 illustrates the importance of incorporating amplitude coordinates in model reduction strategies for jet-lag treatment. The mathematical approach behind the proposed optimal control strategy is presented in Chapter 4 including how the cost functional is derived and how the calculus of variations approach is used as a baseline for formulating the optimal control strategy. The overall methodology and application of the optimal control strategy is illustrated through a 2-d model in Chapter 5 followed by the conclusion in Chapter 6.

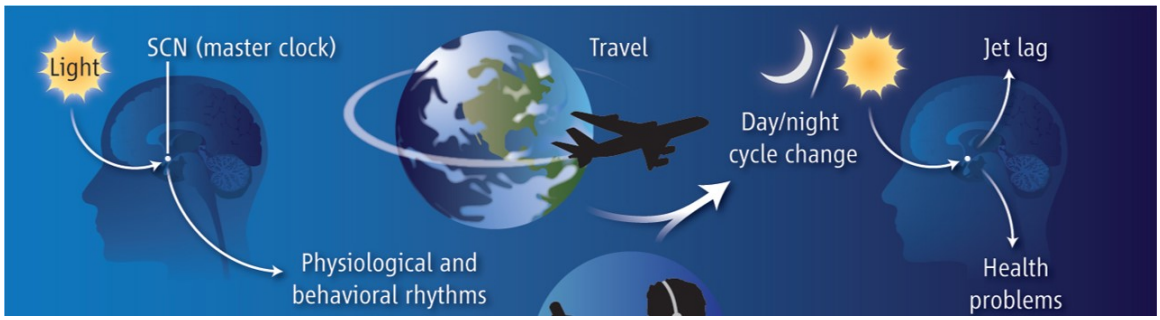

Figure 1.1: How jet-lag is caused [26]

Chapter 2

Background and Literature Review

This chapter starts by a detailed section based upon introducing other jet-lag treatment strategies found in literature and elaborating on each of them briefly. Furthermore, as mentioned in the Introduction chapter, operational phase and isostable reduction framework [69] is used in this work. Therefore, necessary background needs to be provided in order to help understand how these operational phase-amplitude coordinates are derived. Phase-based model reduction is often an initial step in the analysis of many circadian models as they are generally high-dimensional and non-linear in nature. Therefore, the next section in this chapter gives a brief introduction on the phase-only reduction to summarize how exactly the model can be represented in terms of the phase coordinate. The following section touches on the notion of phase amplitude coordinates and how the idea of isostable coordinates is augmented with the phase-only reduction. Finally, the last section illustrates how the standard phase amplitude coordinates can be transformed into operational phase amplitude coordinates to be used in the jet-leg treatment strategy.

2.1 Literature Review

As mentioned in the introductory chapter, a wide variety of methods have already been proposed and used in previous works for jet-lag treatment. Authors in [18] do an extensive study on how rapid level through multiple time zones cause jet-lag and construct one-dimensional entrainment maps to explain several properties and characteristics of jet-lag

including the reason for people experiencing worse implications through jet-lag during eastward travel. Finally, they propose some techniques in order to minimize these deleterious effects by using the insights gained from their analysis. Meanwhile, a study conducted in [29] proposes the use of Argonne diet as a safe and low-cost treatment for jet-lag by advising to follow a strict feasting pattern before and after travel. The preliminary results presented in the paper indicates more frequent instances of jet-lag for non-dieters as compared to those on a diet. Research conducted by the authors in [78] concludes that vasopressin hormone signalling in the Suprachiasmatic nucleus (SCN) can hinder reentrainment to changes in the environmental time. This is supported by an experiment conducted by them on mice that had their vasopressin receptors inhibited; the study shows that these mice have an accelerated recovery from jet-lag.

The work in [17] employs mathematical models derived for the circadian pacemaker to design and alter sleep schedules and other countermeasures in order to accelerate recovery from circadian misalignment and improve performance. This scheduling typically involves factors including, but not limited to, light exposure and sleep-wake schedule; the authors propose that their presented strategies can be utilized for designing optimal schedules to avoid the harmful effects of jet-lag in extreme environments. Another work [19] suggests strategies to minimize jet-lag occurrences by utilizing treatments based on melatonin ingestion, exposure to light and sleep schedules in conjunction with the flight times one has and their overall itinerary. Researchers in [62] explore similar techniques by suggesting appropriate schedules for using conventional jet-lag treatment strategies based on melatonin and light exposure so that the efficacy of these methods can be maximized and the overall health can be improved.

On the other hand, phase-based techniques have been gaining prominence in recent years to tackle issues like jet-lag. For example, [37] utilizes a detailed computational model that predicts the presence of a threshold separating the orthodromic from antidromic re-entrainment. Using the notion of phase response curves, their proposed strategy then predicts the exact location of the aforementioned threshold after advanced or delayed phase shifts of the light-dark cycle. Another work [43] presents an algorithm involving the concepts of isostables and isochrons to represent the model and then use it in conjunction with spike

timing control in order to deal with issues associated with jet-lag among other applications. Finally, authors in [39] do model reduction for the forced Kuramoto model and use biological experiments to estimate its parameters before examining the phase dynamics of the model and study the mechanism for jet-lag resulting from both eastward and westward travel along with differences between the two.

It is pertinent to note here that all of the previous methods either rely on following complex schedules for rapid reentrainment to the new time zone or rely on phase dynamics alone which usually do not consider dynamics far from the periodic orbit. The following sections describe the phase reduction in more detail as well as the ideas behind the standard and operational phase amplitude coordinates.

2.2 Phase-only Reduction

As described previously, given the complexity and high-dimensionality of many circadian models, phase-based model reduction is often a necessary first step in the analysis and identification of jet-lag mitigation strategies. From a mathematical perspective, many models used to study circadian physiology can be written as a set of differential equations of the form

$$\dot{x} = F(x, p(t)), \tag{2.1}$$

where $x \in \mathbb{R}^N$ is the system state, F represents the nominal dynamics, and $p \in \mathbb{R}$ is a (potentially) time-varying parameter that can be used to incorporate features such as a 24-hour light-dark cycle. When $p(t) = p_0$ where p_0 is some nominal, constant parameter, circadian models of the general form (2.1) usually admit a stable, T-periodic limit cycle $x^\gamma(t)$. Letting the phase, θ, be defined according to the notion of isochrons [23], [76] which is also presented in Fig 2.1 so that initial conditions with the same asymptotic convergence to the periodic orbit have the same phase. The dynamics can be analyzed in a phase reduced form [34], [76], [59]

$$\dot{\theta} = \omega + Z_E(\theta)u(t), \tag{2.2}$$

where $Z_E(\theta) = \frac{\partial \theta}{\partial x} \cdot \frac{\partial F}{\partial p}$ is the effective phase response curve (PRC) with all partials evaluated at $x^\gamma(\theta)$ on the limit cycle, and $u(t) = p(t) - p_0$ is an effective input.

2.3 Asymptotic Phase and Isostable Reduction

The operational phase coordinate framework [69] is based on the phase-isostable coordinate framework proposed in [75] (cf., [68], [57]). A brief description of this phase-isostable coordinate framework is presented here. To begin, consider a general dynamical system of the form (2.1) with a T-periodic limit cycle $x^\gamma(t)$ that emerges taking $p(t) = p_0$. When $p(t)$ is held constant at this nominal value, one can define a phase $\theta \in [0, 2\pi)$ valid for all locations on the limit cycle and scaled so that $d\theta/dt = 2\pi/T = \omega$. One can define phase in the entire basin of attraction of the limit cycle using the notion of isochrons as shown in Fig 2.1 [23],[76]. Isochrons are defined such that when $p(t) = p_0$, for any initial condition $a(0) \in x^\gamma(t)$, the isochron associated with $a(0)$ is defined to be the set of all $b(0)$ such that

$$\lim_{t \to \infty} ||a(t) - b(t)|| = 0, \tag{2.3}$$

where $|| \cdot ||$ can be any vector norm. The isochron-based definition of phase encodes for the infinite time behavior of solutions that have been perturbed from the limit cycle. In many situations, it is also useful to consider the amplitude dynamics that capture the transient decay of solutions towards the periodic orbit. In order to leverage Floquet theory [28], one can first define $\Delta x(t) = x(t) - x^\gamma(t)$ so that to a linear approximation, the dynamics of Equation (2.1) are

$$\Delta \dot{x} = J \Delta x, \tag{2.4}$$

where J is the time-varying Jacobian of F evaluated at both $x^\gamma(t)$ and $p = p_0$. Letting Φ be the fundimental matrix defined such that $\Delta x(T) = \Phi \Delta x(0)$, consider the eigenvalues and associated left and right eigenvectors of Φ denoted by λ_j, w_j, and v_j, respectively. Letting λ_1 be the nonunity eigenvalue (i.e., Floquet multiplier) of largest magnitude, it is possible to define a set of isostable coordinates valid in the basin of attraction of the limit cycle according to [68]; this is also illustrated in Fig 2.2.

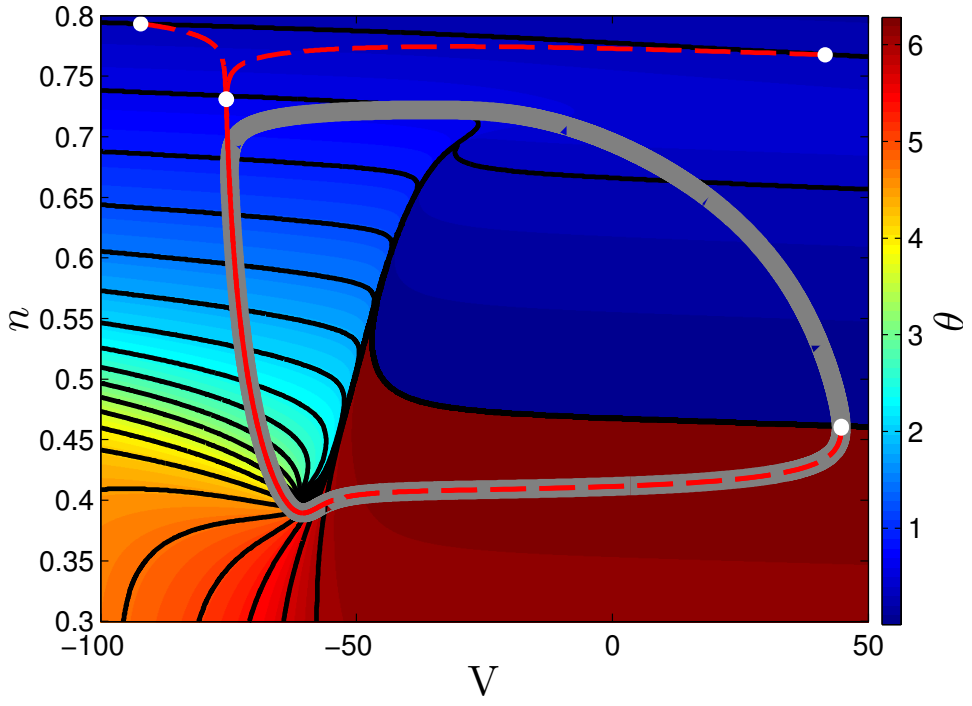

Figure 2.1: Defining phase through isochrons [73]

$$\psi_1(x) = \lim_{k\to\infty} \left[w_1^T(\nu(t_\Gamma^k, x) - x_0) \exp(-\kappa_1 t_\Gamma^k) \right], \tag{2.5}$$

where t_Γ^k denotes time of the k^{th} transversal of the $\theta = 0$ isochron, $\nu(t, x)$ gives the unperturbed flow of Equation (2.1), x_0 is the intersection of the periodic orbit and the $\theta = 0$ isochron, and $\kappa_1 = \log(\lambda_1)/T$ is the associated Floquet exponent. Intuitively, the term $w_1^T(\nu(t_\Gamma^k, x) - x_0)$ captures the exponential decay toward the periodic orbit and the term $\exp(-\kappa_1 t_\Gamma^k)$ grows at a corresponding rate. In the limit as time approaches infinity, the term inside the brackets of (2.5) converges to the isostable coordinate associated with the state x. In general, a collection of isostable coordinates can be defined for the N-dimensional system (2.1), however, it is not always possible to provide an explicit definition like the one from (2.5). Instead, one can define a collection of isostable coordinates $\psi_1, \ldots, \psi_{M-1}$ implicitly as level sets of Koopman eigenfunctions associated with the nonunity Floquet multipliers of the linearized dynamics. More details about the relationship of isostable coordinates to the Koopman operator can be found in [35], [40]. In the basin of attraction of the limit cycle, all isostable coordinates decay exponentially according to $\dot{\psi}_j = \kappa_j \psi_j$ in the absence of perturbation where $\kappa_j = \log(\lambda_j)/T$.

In the absence of other assumptions, the use of isochrons and isostable coordinates on its own does not yield any meaningful simplification of the system dynamics since the phase still depends on the state. However, by assuming that both $p(t) - p_0$ and $x - x^\gamma(t)$ are order ϵ terms at all times where $0 < \epsilon \ll 1$, one can asymptotically expand Equation (2.1) about $x^\gamma(t)$ to yield

$$\begin{aligned} \dot{x} &= F(x, p_0) + \frac{\partial F}{\partial p}(p(t) - p_0) + O(\epsilon^2) \\ &= F(x, p_0) + U(t) + O(\epsilon^2), \end{aligned} \tag{2.6}$$

where the partial derivative is evaluated at both $x^\gamma(t)$ and p_0 and $U(t) \in \mathbb{R}^N = \frac{\partial F}{\partial p}(p(t) - p_0)$. Changing to phase and isostable coordinates via the chain rule as in [75], [68] gives

$$\dot{\theta} = \omega + Z(\theta)^T U(t) + O(\epsilon^2), \tag{2.7}$$

$$\dot{\psi}_j = \kappa_j \psi_j + I_j(\theta)^T U(t) + O(\epsilon^2), \tag{2.8}$$

$$j = 1, \ldots, N-1,$$

where $Z(\theta)$ and $I_j(\theta)$ are the gradients of θ and ψ_j, respectively, (i.e., the phase and isostable response curves). Numerical techniques based on the adjoint method of solution for computing these response curves are described in [75], [7]. It is often possible to ignore isostable coordinates ψ_j for which the corresponding Floquet exponents κ_j are large in magnitude so that they decay rapidly [43], [70], [67]; in this case, the resulting set of equations is of lower order than the original set of equations. Note that to leading order accuracy, the phase dynamics are uncoupled from the isostable dynamics; however, this is not generally true for higher order accuracy phase-amplitude reductions as explored and evaluated in detail in [65] and [68].

In this thesis, a slightly different construction for the phase and isostable equations of the form (2.7) and (2.8) is used:

$$\dot{\theta} = \omega + z(\theta)u(t), \tag{2.9}$$

$$\dot{\psi}_j = \kappa_j \psi_j + i_j(\theta)u(t), \tag{2.10}$$

$$j = 1, \ldots, N-1,$$

where $z(\theta) \in \mathbb{R} = Z(\theta)^T \frac{\partial F}{\partial p}$, each $i_j(\theta) \in \mathbb{C} = I_j(\theta)^T \frac{\partial F}{\partial p}$, and $u(t) = p(t) - p_0$ with partial derivatives evaluated at $x^\gamma(\theta)$ and p_0. Considering the definition of $U(t)$ given directly below (2.6), one can verify that the phase and isostable dynamics from (2.9) and (2.10) are equivalent to those from (2.7) and (2.8).

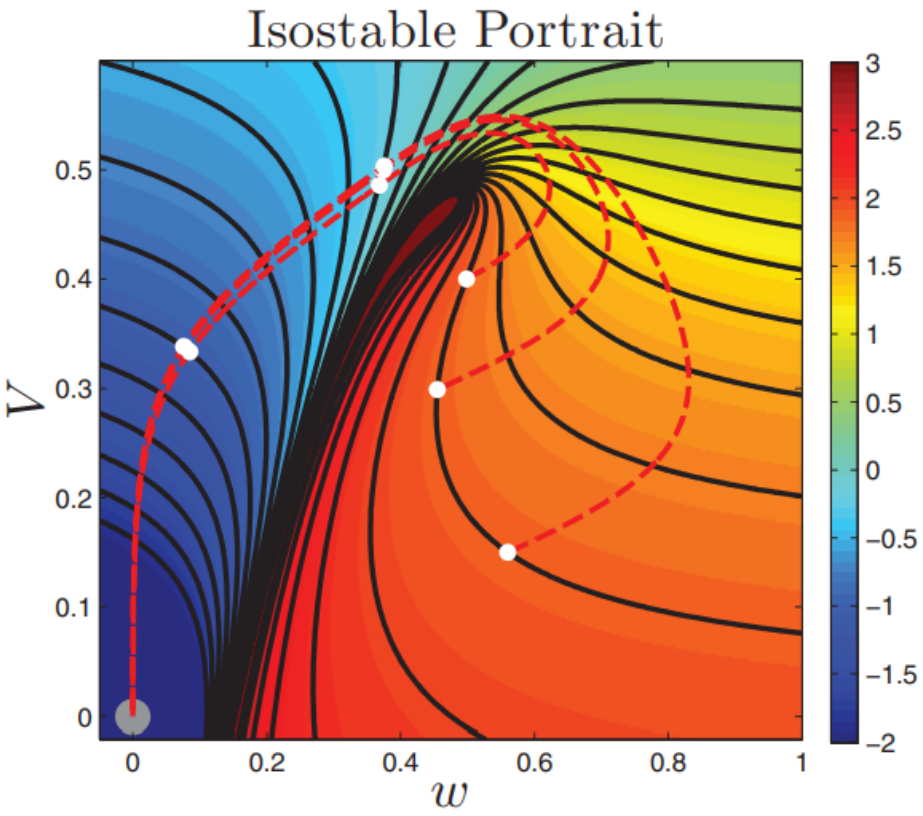

Figure 2.2: Idea of isostable coordinates [74]

2.4 Operational Phase Reduction

Defining phase in terms of the isochrons (2.3) encodes for asymptotic behavior, i.e., the oscillation timing after the state relaxes to the limit cycle. In many applications, however, including those that involve entrainment of circadian oscillators, external inputs are constantly applied and the state never reaches to the limit cycle. In these cases, standard phase-amplitude reduction may not adequately capture the behavior of the full system. With this in mind, as in [69], an operational phase coordinate, $\theta^* \in [0, 2\pi)$, can be used that explicitly defines $\theta^* = 0$ to correspond to some feature of interest near the limit cycle; this idea is portrayed in Fig 2.3. For example, $\theta^* = 0$ can be defined as the time that a periodically spiking neuron fires an action potential, elevating its transmembrane voltage beyond its resting level. Intuitively, such a threshold can be represented as Poincaré section [64], with the time required to start at and return to $\theta^* = 0$ corresponding to the return time. When using operational phase coordinates, $\theta^* = 0$ can be distinctly measured on each cycle, even when the state is far from the periodic orbit. By contrast, the asymptotic phase, θ, can generally only be measured after an oscillator is allowed to relax to the limit cycle in the absence of any exogenous inputs.

The operational phase coordinate, $\theta^*(x)$, can be directly related to the phase and isostable coordinates from Equations (2.7) and (2.8). Following the construction from [69], let $x^\gamma(\theta)$ be a limit cycle where θ is the asymptotic phase. Letting x_k^γ and x_k be the k^{th} element of $x^\gamma(\theta)$ and x, respectively, the $\theta^*(x) = 0$ level set can be defined as all states in the neighborhood of $x^\gamma(0)$ for which both $x_k = x_k^\gamma(0)$ and $\text{sign}\left(\frac{dx_k}{dt}|_x\right) = \text{sign}\left(\frac{dx_k}{dt}|_{x^\gamma(0)}\right)$. As discussed in [69], by leveraging the isostable coordinate framework, the definition of operational phase can be extended to a neighborhood of the limit cycle. The subsequent operational phase and isostable coordinate dynamics of Equation (2.6) are of the form

$$\begin{aligned}
\dot{\theta}^* &= \omega + \sum_{j=1}^{N-1}(\alpha_j \psi_j) + Z^*(\theta^*)^T U(t) + O(\epsilon^2), \\
\dot{\psi}_i &= \kappa_i \psi_i + I_i^*(\theta^*)^T U(t) + O(\epsilon^2), \\
i &= 1, \ldots, N-1,
\end{aligned} \tag{2.11}$$

where constants $\alpha_j \in \mathbb{C}$ characterize how $\dot{\theta}^*$ changes as the state is perturbed from the limit cycle, and $Z^*(\theta^*)$ (resp., $I^*(\theta^*)$) give the gradient of the operational phase and isostable coordinate evaluated at θ^* on the limit cycle. Rewriting (2.11) in a similar form as (2.9) and (2.10) to emphasize the parameter perturbations yields

$$\begin{aligned}
\dot{\theta}^* &= \omega + \sum_{j=1}^{N-1}(\alpha_j \psi_j) + z^*(\theta^*)u(t), \\
\dot{\psi}_i &= \kappa_i \psi_i + i_i^*(\theta^*)u(t), \\
i &= 1, \ldots, N-1,
\end{aligned} \tag{2.12}$$

where $z^*(\theta^*) \in \mathbb{R} = Z^*(\theta^*)^T \frac{\partial F}{\partial p}$, each $i_j^*(\theta^*) \in \mathbb{C} = I_j^*(\theta^*)^T \frac{\partial F}{\partial p}$, and $u(t) = p(t) - p_0$ with partial derivatives evaluated at $x^\gamma(\theta)$ and p_0.

As shown in [69], the phase and isostable response curves from (2.11) are related to those from the phase-isostable reduced equations from (2.7) and (2.8) according to

$$\begin{aligned}
Z^*(\theta^*) &= Z(\theta^*) + \sum_{j=1}^{N-1}\left(\frac{\alpha_j I_j(\theta^*)}{\kappa_j}\right), \\
I_i^*(\theta^*) &= I_i(\theta^*),
\end{aligned} \tag{2.13}$$

for each $i = 1, \ldots, N-1$. Furthermore,

$$\alpha_i = \frac{\omega \kappa_j p_i^{x_k}(0)}{\dot{x}_k(0)}, \tag{2.14}$$

for each $i = 1, \ldots, N-1$ where $p_j^{x_k}(0)$ is k^{th} element of the Floquet eigenfunction associated with ψ_i evaluated at $\theta = 0$ and $\dot{x}_k(0)$ is the time derivative of the k^{th} component of x evaluated at $\theta = 0$ on the limit cycle. To leading order accuracy, an explicit relationship between the operational and asymptotic phase can also be obtained:

$$\theta = \theta^* - \sum_{j=1}^{N-1}\frac{\alpha_j \psi_j}{\kappa_j}. \tag{2.15}$$

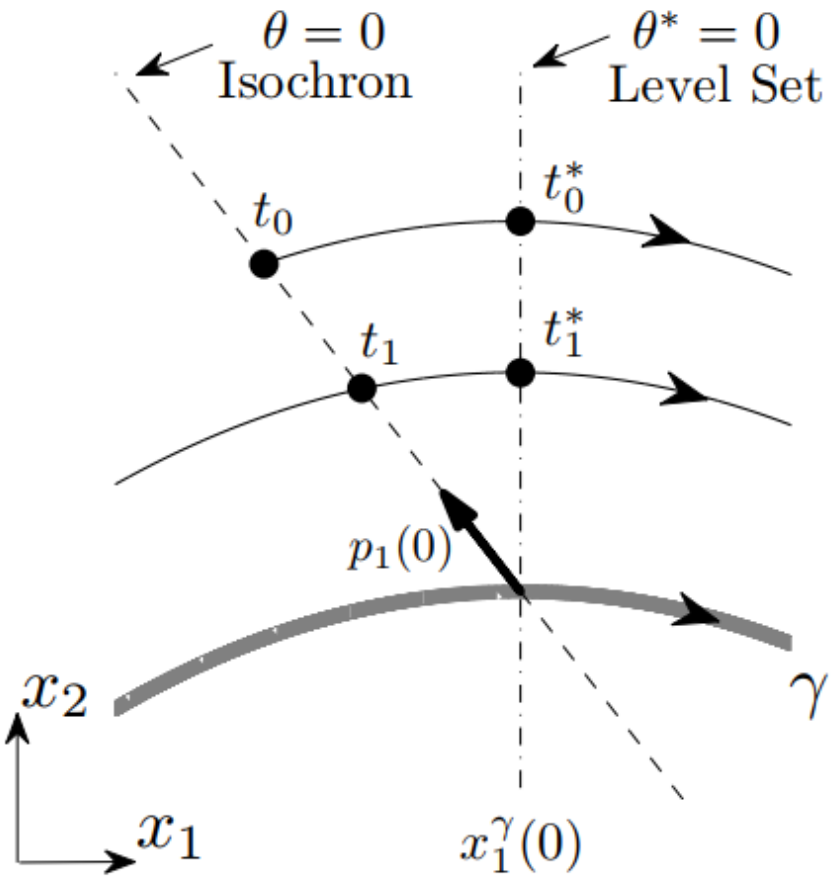

Figure 2.3: Concept of operational phase [69]

Chapter 3

Motivation Behind Considering Amplitude Coordinates

In order to illustrate the fundamental importance of amplitude coordinates in applications involving reentrainment, a modified version of the radial isochron clock from [76] is considered.

$$\begin{aligned}\dot{x} &= \frac{2\pi}{T}\left[\sigma x(1-x^2-y^2) - y(1+\rho(x^2+y^2-1))\right] + f_e(t),\\ \dot{y} &= \frac{2\pi}{T}\left[\sigma y(1-x^2-y^2) + x(1+\rho(x^2+y^2-1))\right],\end{aligned} \tag{3.1}$$

where x and y are spatial coordinates and $f_e(t)$ is an entraining stimulus. When $f_e(t) = 0$ and $\rho > 0$, Equation (3.1) has a stable limit cycle that traces out a unit circle with period T. The constant $\rho = 0.12$ determines how the radial distance from the periodic orbit influences the rate of revolution and $\sigma = 0.04$ sets the relaxation rate to the periodic orbit. For this specific example, the time period and the entraining stimulus are $T = 24.2$ hours and $f_e(t) = 0.025\sin(2\pi t/24 + 0.58)$. These values are chosen to reflect the relationship between the free-running period of a circadian oscillator (slightly longer than 24 hours [13], [8]) and an exogenous 24-hour signal (such as a light-dark cycle) to which the oscillator can entrain. Under the application of $f_e(t)$, all initial conditions converge to an entrained solution shown as a solid black line in panel A of Figure 3.1. When the oscillator is entrained and $\mathrm{mod}(t, 24) = 0$, $(x, y) = (1.12, 0)$ (green dot). Colored dots represent initial conditions on the

entrained solution for which the external time has been shifted by Δt hours (e.g., as a result of a flight across one or more time zone). Open and closed circles correspond to positive and negative values of Δt, respectively. Subsequent reentrainment to the time-shifted stimulus is illustrated in panels B and C. In general, reentrainment time increases as Δt becomes larger in magnitude.

In panel A of Fig 3.1, the unperturbed periodic orbit (i.e., with $f_e(t) = 0$) is shown as a dashed line. Under the application of $f_e(t)$, the resulting fully entrained solution is shown in black. Colored dots represent initial conditions on the periodic orbit for which time (and the resulting perturbation $f_e(t)$) has suddenly been shifted to $\mathrm{mod}(t, 24) = 0$, mimicking a time zone change due to rapid travel. Open and closed circles represent initial conditions on the entrained solution which have been shifted forward or backwards in time, respectively. Panel B shows $x(t)$ during subsequent reentrainment for each initial condition. In panel C, $\mu(t)$ is the angle in a radial coordinate system, and $\mu_{\mathrm{ref}}(t)$ is the angle of the fully entrained solution.

Figure 3.1 illustrates how reentrainment time depends strongly on the magnitude of the time shift and corresponding misalignment in the angular direction. However, the radial direction also has a strong influence on reentrainment as can be seen in the colormap in panel A of Figure 2. Panels B and C in Fig. 2 show corresponding simulations illustrating how the radial coordinate influences reentrainment: a larger radial coordinate results in more rapid reentrainment following a +6 hour time shift while the same increased radial coordinate delays reentrainment after a -6 hour shift. This discrepancy exists despite the fact that each oscillator receives the same input $f_e(t)$ in each trial.

Meanwhile in Fig 3.2, Panel A shows the time for various initial conditions required to achieve entrainment to the input $f_e(t)$ starting at $t = 0$. In polar coordinates, taking $\mu_{\mathrm{ref}}(t)$ to be the angular coordinate associated with the fully entrained solution, the recovery time t_{rec} is defined to be the largest t for which $|\mu(t) - \mu_{ref}(t)| > 0.26$, corresponding to a 1 hour time difference. Open and closed circles represent initial conditions on the entrained solution which have been shifted forward or backwards in time, respectively. Panel B (resp., C) shows the recovery of initial conditions which are initially $-\pi/2$ (resp., $\pi/2$) radians out of phase

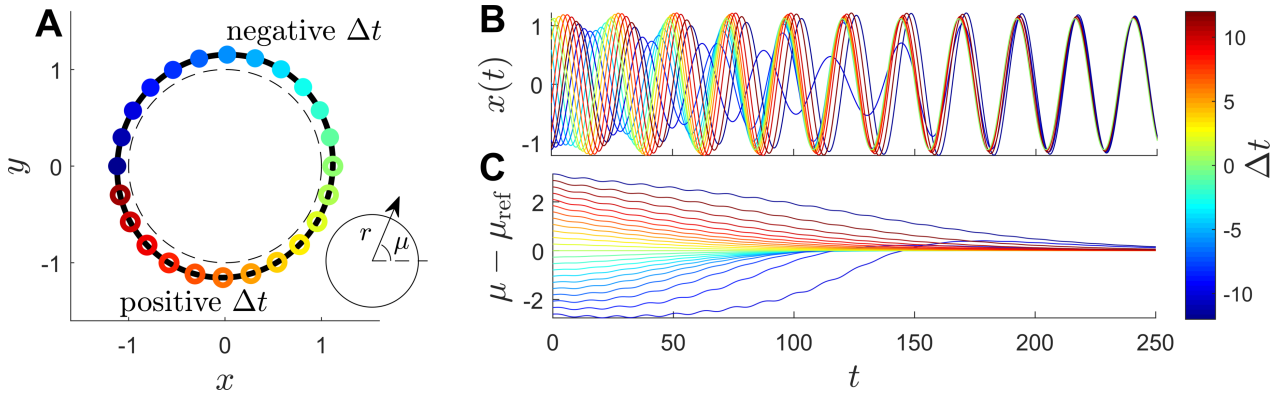

Figure 3.1: Effect of time shift on the entrained solution [1]

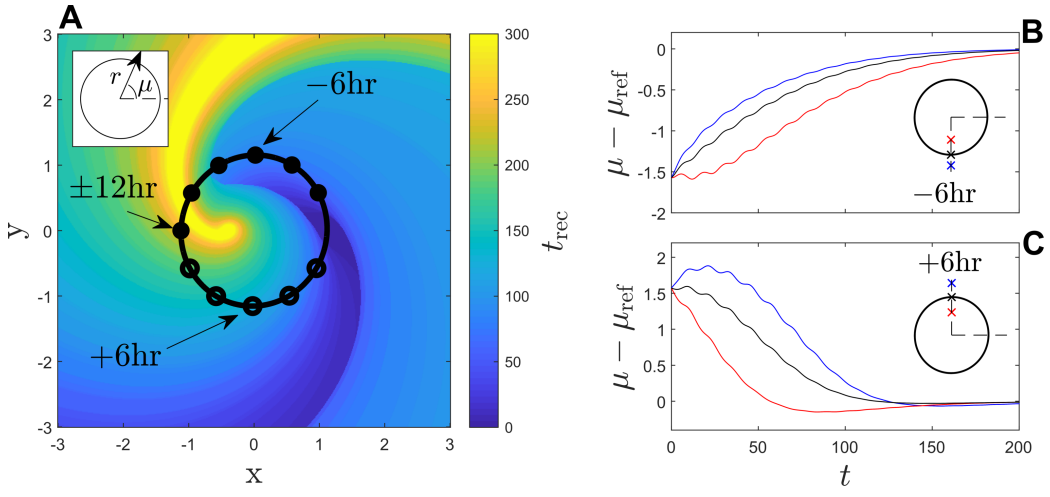

Figure 3.2: How varying radial coordinates influences recovery times [1]

due to a $+6$ (resp., -6) hour time shift. In each example, the radial direction significantly influences the recovery time.

As explained above, by shifting the state in the radial direction only, it is possible to either hasten or delay recovery times. Motivated by this fact, in the chapter to follow, a jet-lag pretreatment strategy is proposed and evaluated that seeks to optimally shift the amplitude coordinate in order to hasten circadian reentrainment following an expected time shift. In contrast to many jet-lag recovery strategies that just consider the phase dynamics of reduced order models, the use of the operational phase-amplitude coordinate framework allows to exploit circadian memory to achieve this goal.

Chapter 4

Proposed Optimal Control Method for Shifting Amplitude Coordinates

As stated in the Introduction, an optimal control strategy for optimally shifting only the amplitude coordinates associated with a periodic orbit is presented in this chapter. As mentioned earlier in the thesis, when larger magnitude amplitude coordinates are considered, the asymptotic phase from (2.9) does not, in general, accurately capture salient system behaviors. For this reason, the operational phase and isostable framework from Equation (2.12) is employed.

4.1 Identifying an Appropriate Cost Functional

Here, an optimal control problem for a general model of the form (2.1) is posed that can be represented in terms of its operational phase and isostable dynamics using a model of the form (2.12). In the derivation to follow, it is assumed that there are $\beta < N-1$ non-truncated isostable coordinates yielding the reduced order model

$$\begin{aligned}
\dot{\theta}^* &= \omega + \sum_{i=1}^{\beta} (\alpha_i \psi_i) + \epsilon z^*(\theta^*)(u(t) + u_e(t)), \\
\dot{\psi}_i &= \kappa_i \psi_i + \epsilon i_i^*(\theta^*)(u(t) + u_e(t)), \\
i &= 1, \ldots, \beta.
\end{aligned} \tag{4.1}$$

Above, the overall input is comprised of the control input, $u(t)$, and a nominal entraining stimulus, $u_e(t)$, (for instance, a 24-hour light-dark cycle). Also, it is explicitly assumed that the overall input is an order ϵ term where $0 < \epsilon \ll 1$. Furthermore, the entraining stimulus u_e is assumed to be T_e-periodic. Letting $\omega_e = 2\pi/T_e$, it is also assumed that $\omega - \omega_e$ is an order ϵ term, i.e. so that the entrained period is close to the natural period. Finally, as illustrated in Appendix C of [70], provided the input is an order ϵ term and sufficiently small relative to each Floquet exponent, each isostable coordinate is also an order ϵ term. Consider for the moment the stable, fully entrained solution of (4.1) that results in the limit as time approaches infinity when $u(t) = 0$. The associated operational phase and isostable dynamics on this fully entrained solution, $\theta_e^*(t)$ and $\psi_{i,e}(t)$, respectively, follow

$$\begin{aligned}
\dot{\theta}_e^* &= \omega + \sum_{i=1}^{\beta} (\alpha_i \psi_{i,e}) + \epsilon u_e(t) z^*(\theta_e^*), \\
\dot{\psi}_{i,e} &= \kappa_i \psi_{i,e} + \epsilon i_i^*(\theta_e^*) u_e(t), \\
i &= 1, \ldots, \beta.
\end{aligned} \tag{4.2}$$

To proceed, for any initial condition $\theta(0)^* = \theta_e^*$, letting $\Delta\theta^* = \theta^* - \theta_e^*$ and $\Delta\psi_i = \psi_i - \psi_{i,e}$, one finds

$$\begin{aligned}
\Delta\dot{\theta}^* &= \dot{\theta}^* - \dot{\theta}_e^* \\
&= \sum_{i=1}^{\beta} \alpha_i \Delta\psi_i + \epsilon z^*(\theta^*) u(t) + \epsilon u_e(t)[z^*(\theta^*) - z^*(\theta_e^*)] + \mathcal{O}(\epsilon^2) \\
&= \sum_{i=1}^{\beta} \alpha_i \Delta\psi_i + \epsilon z^*(\theta^*) u(t) + \epsilon u_e(t) z^{*\prime}(\theta_e^*) \Delta\theta^* + \mathcal{O}(\Delta\theta^{*2}) + \mathcal{O}(\epsilon^2),
\end{aligned} \tag{4.3}$$

where $' \equiv \frac{d}{d\theta^*}$. Noticing that all terms of $\Delta\dot{\theta}^*$ are order ϵ terms, $\Delta\theta^*$ is an order ϵ term on $t \sim \mathcal{O}(1/\epsilon)$. As such, we can rewrite (4.3) as

$$\Delta\dot{\theta}^* = \sum_{i=1}^{\beta} \alpha_i \Delta\psi_i + \epsilon z^*(\theta^*) u(t) + \mathcal{O}(\epsilon^2). \tag{4.4}$$

In a similar manner, considering Equations (4.1) and (4.2), the dynamics of each isostable coordinate follow

$$\begin{aligned}\Delta\dot{\psi}_i &= \kappa_i\Delta\psi_i + \epsilon i_i^*(\theta^*)u(t) + \epsilon[i_i^*(\theta^*) - i_i^*(\theta_e^*)]u_e(t) + \mathcal{O}(\epsilon^2)\\ &= \kappa_i\Delta\psi_i + \epsilon i_i^*(\theta^*)u(t) + \epsilon u_e(t)i^{*\prime}(\theta_e^*)\Delta\theta^* + \mathcal{O}(\Delta\theta^{*2}) + \mathcal{O}(\epsilon^2)\\ &= \kappa_i\Delta\psi_i + \epsilon i_i^*(\theta^*)u(t) + \mathcal{O}(\epsilon^2),\end{aligned} \tag{4.5}$$

for $i = 1, \ldots, \beta$.

Equations (4.4) and (4.5) will be used as a foundation in the following optimal control formulation. For the formulation, the initial condition is considered such that it is fully entrained to $u_e(t)$ at $t = 0$ with associated operational phase and isostable coordinates $\theta^*(0) = \Delta\theta^*(0) = 0$ and $\Delta\psi(0) = 0$. Suppose that at $t = T_e$ (i.e., after the entraining stimulus has been applied for one cycle), the external timing of the entraining stimulus suddenly shifts by Δt, more precisely,

$$u_e(t) = u_e(t + h(T_e)\Delta t), \tag{4.6}$$

where h is the unit step function. An input $u(t)$ needs to be obtained, applied over $t \in [0, T_e]$, that will prime the system for recovery from the resulting misalignment by appropriately influencing the isostable coordinates. To this end, all inputs $u(t)$ that yield $\Delta\theta^*(T_e) = 0$ are considered, in other words, the set of all inputs that have no net influence on the operational phase. Depending on whether Δt is positive or negative, an optimal stimulus is derived that minimizes the cost functional

$$C = \begin{cases} \int_0^{T_e} X\epsilon^2 u^2(t)dt - (1-X)\sum_{i=1}^{\beta}\left(-\frac{\alpha_i\Delta\psi_i(T_e)}{\kappa_i}\right), & \text{if } \Delta t > 0,\\ \int_0^{T_e} X\epsilon^2 u^2(t)dt + (1-X)\sum_{i=1}^{\beta}\left(-\frac{\alpha_i\Delta\psi_i(T_e)}{\kappa_i}\right), & \text{if } \Delta t < 0.\end{cases} \tag{4.7}$$

Here, the term $\int_0^{T_e}\epsilon^2 u^2(t)dt$ is the L^2 norm of the input $\epsilon u(t)$, which gives a sense of the control effort. Terms of the form $-\frac{\alpha_j\Delta\psi_j(T_e)}{\kappa_j}$ appropriately reward a latent phase shift that can be used to hasten resynchronization. To see this, considering Equation (4.5) to leading order ϵ, $\Delta\psi_j(t) = \Delta\psi_j(T_e)\exp(\kappa_j(t - T_e))$ in the absence of input. As such, the total

operational phase shift once the state relaxes back to the limit cycle will be

$$\lim_{t\to\infty} \Delta\theta^*(t) = \int_{T_e}^{\infty} \left[\sum_{i=1}^{\beta} \alpha_i \Delta\psi_i(T_e) \exp(\kappa_i(t - T_e)) \right] dt$$
$$= \sum_{i=1}^{\beta} -\frac{\alpha_i \Delta\psi_i(T_e)}{\kappa_i}. \tag{4.8}$$

As such, shifting the isostable coordinates can prime the underlying system (2.1) to respond appropriately to an expected shift in the environmental time. For instance, taking $\Delta t > 0$, the overall cost is decreased when the latent phase is positive, ultimately hastening resynchronization. Finally, $X \in (0, 1]$ is a weighting term that sets the relative importance of minimizing energy versus shifting the isostable coordinate.

4.2 A Calculus of Variations Approach for Minimizing the Cost Functional

Following a calculus of variations approach [32], the Hamiltonian function associated with the cost functional (4.7) is

$$H(y(t), u(t), p(t), t) = X\epsilon^2 u^2(t) + \lambda_0 \big[\sum_{i=1}^{\beta} (\alpha_i \Delta\psi_i) + \epsilon z^*(\theta^*) u(t) \big]$$
$$+ \sum_{i=1}^{\beta} \lambda_i [\kappa_i \Delta\psi_i + \epsilon i_i^*(\theta^*) u(t)], \tag{4.9}$$

where $y \equiv \begin{bmatrix} \Delta\theta^* & \Delta\psi_1 & \dots & \Delta\psi_\beta \end{bmatrix}^T$, and $p \equiv \begin{bmatrix} \lambda_0 & \dots & \lambda_\beta \end{bmatrix}^T$ are Lagrange multipliers. The associated Euler-Lagrange equations are

$$\dot{y} = \frac{\partial H}{\partial p}, \tag{4.10}$$
$$\dot{p} = -\frac{\partial H}{\partial y}, \tag{4.11}$$
$$0 = \frac{\partial H}{\partial u}. \tag{4.12}$$

The evaluation of (4.10) yields the state equations (4.4) and (4.5). Evaluation of (4.11) yields

$$\dot{\lambda}_0 = -\epsilon z^{*\prime}(\theta^*)u(t)\lambda_0 - \sum_{i=1}^{\beta}\left(\epsilon i_i^{*\prime}(\theta^*)u(t)\lambda_i\right),$$
$$\dot{\lambda}_i = -\lambda_i\kappa_i - \alpha_i\lambda_0. \tag{4.13}$$

Finally, evaluation of (4.12) yields

$$u(t) = \frac{-\lambda_0 z^*(\theta^*) - \sum_{i=1}^{\beta}\lambda_i i_i^*(\theta^*)}{2\epsilon X}. \tag{4.14}$$

Equations (4.4), (4.5), (4.13), and (4.14) comprise a set of $2(\beta+1)$ Euler-Lagrange equations that must be satisfied along extremal solutions. $\beta+2$ of the required boundary conditions, $\Delta\theta^*(0) = \Delta\theta^*(T_e) = \Delta\psi_1(0) = \cdots = \Delta\psi_\beta(0) = 0$, have already been specified by the problem formulation. Noting that the final states of the isostable coordinates $\Delta\psi_1(T_e), \ldots, \Delta\psi_\beta(T_e)$ are free, the remaining boundary conditions can be specified by requiring [32]

$$\left.\frac{\partial g}{\partial \Delta\psi_i}\right|_{t=T_e} - \lambda_i(T_e) = 0, \tag{4.15}$$

for $i = 1, \ldots, \beta$, where $g = -\text{sign}(\Delta t)(1-X)\sum_{i=1}^{\beta}\left(-\frac{\alpha_i\Delta\psi_i}{\kappa_i}\right)$ is used to determine the endpoint cost from (4.7). Evaluating (4.15) yields the remaining boundary conditions

$$\lambda_i(T_e) = \text{sign}(\Delta t)(1-X)\frac{\alpha_i}{\kappa_i}, \tag{4.16}$$

for $i = 1, \ldots, \beta$.

As a matter of practical implementation, obtaining a solution to the above system of Euler-Lagrange equations involves identifying a set of initial values for the Lagrange multipliers, $\lambda_0(0), \ldots, \lambda_\beta(0)$, that yield the required final conditions at time T_e under the evolution of the Euler-Lagrange equations (4.10)-(4.12). This can be accomplished by first noting that when $X = 1$ in the cost functional (4.7), $u(t) = 0$ is the minimal solution with corresponding $\lambda_i(0) = 0$ for $i = 0, 1, \ldots, \beta$. Subsequently, X can be incrementally decreased

and the required Lagrange multipliers at each increment can be obtained using a Newton iteration until the extremal solution for the desired value of X identified.

4.3 An Explicit Formulation of an Approximate Solution to the Optimal Control Problem

The process of finding solutions of the Euler-Lagrange equations (4.10)-(4.12) with the required boundary conditions becomes unwieldy as the number of isostable coordinates, and subsequently the dimensions of the Euler-Lagrange equations, increases. Additionally, it can be difficult to know if the resulting extremal solutions represent globally optimal solutions, or merely locally optimal solutions. Here, an explicit strategy is provided to compute an approximate solution that minimizes the cost functional (4.7) that is valid in the limit that the magnitude of the input is small.

To begin, notice from (4.1) that one can write $\dot{\theta}^* = \omega + \mathcal{O}(\epsilon)$, and recalling that $\theta^*(0) = 0$, one finds

$$\theta^*(t) = \omega t + \mathcal{O}(\epsilon). \tag{4.17}$$

With this in mind, considering the leading order ϵ dynamics of each $\Delta\psi_i$, by first defining $r_i \equiv \Delta\psi_i(t)e^{-\kappa_i t}$ and substituting this into Equation (4.5) one finds

$$\Delta\dot{\psi}_i = \dot{r}_i e^{\kappa_i t} + \kappa_i r_i e^{\kappa_i t} = \kappa_i r_i e^{\kappa_i t} + \epsilon i_i^*(\omega t)u(t). \tag{4.18}$$

Hence,

$$\begin{aligned} \dot{r}_i &= \epsilon e^{-\kappa_i t} i_i^*(\omega t)u(t) \\ r_i(t) &= r(t_0) + \epsilon \int_0^t e^{-\kappa s} i_i^*(\omega s)u(s)ds. \end{aligned} \tag{4.19}$$

Substituting $\Delta\psi_i = r_i e^{\kappa_i t}$ into the above equation and recalling that $\Delta\psi_i(0) = 0$ yields

$$\Delta\psi_i(T_e) = \epsilon \int_0^{T_e} e^{\kappa_i (T_e - s)} i_i^*(\omega s)u(s)ds. \tag{4.20}$$

Substituting the above result into the cost functional from (4.7) gives

$$C = \int_0^{T_e} \left[X\epsilon^2 u^2(t) - \epsilon \text{sign}(\Delta t)(1-X) \sum_{i=1}^{\beta} \big(- \frac{\alpha_i}{\kappa_i} e^{\kappa_i (T_e - t)} i_i^*(\omega t) u(t) \big) \right] dt. \tag{4.21}$$

The goal of the optimization is to find the input $u(t)$ that minimizes (4.21) subject to the constraint $\Delta\theta^*(T_e) = 0$. This constraint can be written in a form similar to (4.21) by considering the asymptotic phase dynamics using an equation of the form (2.9)

$$\dot{\theta} = \omega + \epsilon z(\theta)(u(t) + u_e(t)), \tag{4.22}$$

as well as the asymptotic phase dynamics of the fully entrained solution $\theta_e(t)$ which follows

$$\dot{\theta} = \omega + \epsilon z(\theta_e) u_e(t). \tag{4.23}$$

One can define $\Delta\theta \equiv \theta - \theta_e$ and also note $\theta = \theta^* + \mathcal{O}(\epsilon)$. Using a similar asymptotic expansion used to obtain (4.4), one can show

$$\Delta\dot{\theta} = \epsilon z(\omega t) u(t) + \mathcal{O}(\epsilon^2). \tag{4.24}$$

Noting that at $t = 0$, the system is fully entrained so that $\Delta\theta(0) = 0$, direct integration of (4.24) yields

$$\Delta\theta(T_e) = \int_0^{T_e} \epsilon z(\omega t) u(t) dt. \tag{4.25}$$

Applying (2.15), it can be shown that $\Delta\theta = \Delta\theta^* - \sum_{i=1}^{\beta} (\alpha_i \Delta\psi_i / \kappa_i)$. Using this result to transform (4.25) to operational phase coordinates, the required constraint for the cost functional optimization becomes

$$\begin{aligned} \Delta\theta^*(T_e) = 0 &= \int_0^{T_e} \epsilon z(\omega t) u(t) dt + \sum_{i=1}^{\beta} \frac{\alpha_i \Delta\psi_i(T_e)}{\kappa_i} \\ &= \epsilon \int_0^{T_e} \left[z(\omega t) u(t) + \sum_{i=1}^{\beta} \big(\frac{\alpha_i}{\kappa_i} e^{\kappa_i (T_e - t)} i_i^*(\omega t) u(t) \big) \right] dt, \end{aligned} \tag{4.26}$$

where the second line is obtained by substituting the result from (4.20). Using an optimization approach based on a calculus of variations formulation [32], the integral constraint (4.26) can be rewritten as an ordinary differential equation

$$\frac{dQ}{dt} = \epsilon z(\omega t)u(t) + \epsilon \sum_{i=1}^{\beta} \big(\frac{\alpha_i}{\kappa_i} e^{\kappa_i (T_e - t)} i_i^*(\omega t)u(t)\big), \tag{4.27}$$

with boundary conditions $Q(0) = Q(T_e) = 0$. As such, the Hamiltonian associated with the cost functional (4.21) subject to the constraint from Equation (4.27) is

$$\begin{aligned} H(y, u(t), p, t) = X\epsilon^2 u^2(t) - \epsilon \text{sign}(\Delta t)(1 - X) \sum_{i=1}^{\beta} \big(- \frac{\alpha_i}{\kappa_i} e^{\kappa_i (T_e - t)} i_i^*(\omega t)u(t)\big) \\ + \lambda_1 [\epsilon z(\omega t)u(t) + \epsilon \sum_{i=1}^{\beta} \big(\frac{\alpha_i}{\kappa_i} e^{\kappa_i (T_e - t)} i_i^*(\omega t)\big)u(t)], \end{aligned} \tag{4.28}$$

where $y = Q$ is the state and $p = \lambda_1$ is a single Lagrange multiplier. The Euler-Lagrange equations (4.10)-(4.12) once again can be used to identify extremal solutions. Evaluation of (4.12) yields the input

$$\begin{aligned} u(t) &= \frac{1}{2X\epsilon} \big(\text{sign}(\Delta t)(1 - X) \sum_{i=1}^{\beta} \big(- \frac{\alpha_i}{\kappa_i} e^{\kappa_i (T_e - t)} i_i^*(\omega t)\big) - \lambda_1 [z(\omega t) + \sum_{i=1}^{\beta} \big(\frac{\alpha_i}{\kappa_i} e^{\kappa_i (T_e - t)} i_i^*(\omega t)\big)]\big) \\ &= \lambda_1 u_\lambda(t) + u_0(t), \end{aligned} \tag{4.29}$$

where $u_\lambda(t)$ and $u_0(t)$ are defined appropriately and are simply functions associated with the operational and asymptotic phase reduced equations. Note that $z(\omega t)$ in the above equation is the asymptotic phase response curve and not the operational phase response curve. Continuing to consider the Euler-Lagrange equations for (4.28), evaluation of Equation (4.10) returns (4.27) and evaluation of (4.11) yields

$$\dot{\lambda}_1 = 0. \tag{4.30}$$

As such, λ_1 is a constant. With this information, substituting (4.29) into the constraint (4.26) gives

$$\begin{aligned} 0 &= \epsilon \int_0^{T_e} \left[\left(z(\omega t) + \sum_{i=1}^{\beta} \left(\frac{\alpha_i}{\kappa_i} e^{\kappa_i (T_e - t)} i_i^*(\omega t) \right) \right) \left(u_\lambda(t) \lambda_1 + u_0(t) \right) \right] dt, \\ &= \lambda_1 c_\lambda + c_0, \end{aligned} \tag{4.31}$$

where $c_\lambda = \epsilon \int_0^{T_e} \left(z(\omega t) + \sum_{i=1}^{\beta} \left(\frac{\alpha_i}{\kappa_i} e^{\kappa_i (T_e - t)} i_i^*(\omega t) \right) \right) u_\lambda(t) dt$ and
$c_0 = \epsilon \int_0^{T_e} \left(z(\omega t) + \sum_{i=1}^{\beta} \left(\frac{\alpha_i}{\kappa_i} e^{\kappa_i (T_e - t)} i_i^*(\omega t) \right) \right) u_0(t) dt$ are both constants. Provided $c_\lambda \neq 0$, the unique choice of λ_1 that satisfies the boundary conditions is

$$\lambda_1 = -c_0 / c_\lambda, \tag{4.32}$$

and thus, an explicit approximation of the control input that minimizes the cost functional is

$$u(t) = -\frac{c_0}{c_\lambda} u_\lambda(t) + u_0(t), \tag{4.33}$$

which is valid in the limit that the magnitude of the input is small.

Chapter 5

Methodology and Results

5.1 Adjoint Method

The adjoint method is used in order to derive the Phase Response Curves and Isostable Response Curves for the radial model to be used in conjunction with the optimal control methodology. For the purpose of understanding how the method exactly works, detailed derivation for the adjoint method (taken from [43]) in order to extract the phase response curve is presented in this section. Initially, one considers an infinitesimal perturbation Δx to the limit cycle $x^\gamma(t)$ at time $t = 0$. Let $x(t)$ be the trajectory evolving from the perturbed initial condition. Thus, one can define $x(t)$ according to $x(t) = x^\gamma(t) + \Delta x(t)$ and,

$$\frac{d\Delta x(t)}{dt} = DF(x^\gamma(t))\Delta x(t) + \mathcal{O}(||\Delta x||^2), \tag{5.1}$$

Similarly, one can define the phase shift as $\Delta\theta = \theta(x(t)) - \theta(x^\gamma(t))$ which can also be written as,

$$\Delta\theta = \langle \nabla_{x^\gamma(t)}\theta, \Delta x(t)\rangle + \mathcal{O}(||\Delta x||^2), \tag{5.2}$$

where $\langle ., .\rangle$ defines the standard inner product and $\bigtriangledown_{x^\gamma(t)}\theta$ is the gradient of θ evaluated at $x^\gamma(t)$. It can be inferred from the equations above that $\Delta\theta$ is independent of time specifically after the perturbation applied at $t = 0$ so taking the time derivative of (5.2) to first order i.e. lowest order in $||\Delta x||$,

$$\begin{aligned}\left\langle \frac{d\nabla_{x^\gamma(t)}\theta}{dt}, \Delta x(t) \right\rangle &= -\left\langle \nabla_{x^\gamma(t)}\theta, \frac{d\Delta x(t)}{dt} \right\rangle, \\ &= -\left\langle \nabla_{x^\gamma(t)}\theta, DF(x^\gamma(t))\Delta x(t) \right\rangle, \\ &= -\left\langle DF^T(x^\gamma(t))\nabla_{x^\gamma(t)}\theta, \Delta x(t) \right\rangle \end{aligned} \tag{5.3}$$

Here, the matrix $DF^T(x^\gamma(t))$ is the transpose (adjoint) of the original matrix $DF(x^\gamma(t))$. As the above equation can hold for any arbitrary infinitesimal perturbation $\Delta x(t)$, one can write

$$\frac{d\nabla_{x^\gamma(t)}\theta}{dt} = -DF^T(x^\gamma(t))\nabla_{x^\gamma(t)}\theta, \tag{5.4}$$

The result shown above follows from the non-degeneracy property of the inner product, which states that if $< a, b >= 0$ for all b, then $a = 0$. To emphasize this property, one can rearrange (5.3) as,

$$\left\langle \frac{d\nabla_{x^\gamma(t)}\theta}{dt} + DF^T(x^\gamma(t))\nabla_{x^\gamma(t)}\theta, \Delta x(t) \right\rangle = 0,$$

where $\frac{d\nabla_{x^\gamma(t)}\theta}{dt} + DF^T(x^\gamma(t))\nabla_{x^\gamma(t)}\theta$ can be defined as $a(t)$. Now, if $\Delta x(t)$ is taken to be $a(t)$, the expression will be $\langle a, a \rangle = 0$. and it can be inferred that $a = 0$ from the definite positivity of the inner product, finally resulting in the form shown in (5.4). Note that

$$\frac{d\theta}{dt} = \nabla_x\theta.\frac{dx}{dt} = \nabla_x\theta.F(x) = \omega,$$

which holds true especially at $t = 0$. Thus, (5.4) needs to be solved using the following condition,

$$\nabla_{x^\gamma(0)}\theta.F(x^\gamma(0)) = \omega, \tag{5.5}$$

Since $\nabla_{x^\gamma(t)}\theta$ exists in $\mathcal{R}_n$, (5.5) gives only one of n required initial conditions; the rest arise from requiring that the solution $\nabla_{x^\gamma(t)}\theta$ to (5.4) be T -periodic.

5.2 Method Summary

This section describes how the adjoint method is used to extract the response curves for the non-radial isochron model before they are used to derive the optimal control inputs. As the first step, the model equations are used in order to extract the periodic orbit with starting threshold set at zero for the x component in (3.1). Once the periodic orbit is extracted, the time period for the periodic orbit is calculated and then, the time period value T (24.2 hrs in this case) is used to calculate the value of ω using $\frac{2\pi}{T}$. These computed values are then used in order to generate the Jacobian matrix for the linearization process using numerical integration.

In the next step, the Jacobian matrix is used in order to extract the eigen vectors and eigen values for the linearized system; the eigen values are then sorted in descending order and then used in order to extract the kappa (κ) values (or Floquet exponents). For the non-radial isochron model, a 2×2 Jacobian matrix is obtained; the eigen values are of the magnitude 0.6055 and 1. Similarly, the extracted floquet exponents values are 7.4314×10^{-7} corresponding to the unit eigen value and -0.0207 value corresponding to the other eigen value. Once all the necessary values have been extracted, the adjoint method is used to extract the phase response curve (PRC) and the isostable response curve (IRC). The equations for extracting both the PRC and IRC using numerical integration are given below:

$$\begin{aligned} Z_{d+1} &= J_k Z_d dt + Z_d, \\ I_{d+1} &= J_k * I_d dt - \kappa_j \mathbf{I} I_d dt + I_d \end{aligned} \tag{5.6}$$

where Z_d corresponds to the PRC, I_d is the IRC, J is the Jacobian matrix and $\mathbf{I}$ is the identity matrix. The computed PRC is then normalized in order to ensure that the PRC is accurate for further computations; afterwards, the obtained IRC and PRC is then flipped and scaled accordingly in order to get the final curves . For conversion of the standard PRC and IRC to the operational ones, some additional parameters need to be calculated for getting the value of α as shown in (2.14). The value of p_j comes from the scaled down right eigen vector specifically the first component of the eigen vector corresponding to the isostable coordinate, the value $\dot{x}_k$ represents the time derivative of the first point of the periodic orbit while ω

and κ values are already computed. The computed alpha value comes out to be -0.0014 in this case; using the alpha value, the operational PRC and IRC are computed by:

$$\begin{aligned} I_i^*(\theta^*) &= I_i(\theta), \\ Z^*(\theta^*) &= Z(\theta) + \sum_{j=1}^{N} \left(\frac{\alpha_j I_j(\theta^*)}{\kappa_j} \right) \end{aligned} \tag{5.7}$$

As can be seen from the (5.7), the isostable response curve remains as it is even after conversion to operational phase-amplitude coordinates; meanwhile, the operational PRC is different from the standard PRC. Now, in order to compute the optimal control input, the obtained operational PRC and IRC are interpolated and shifted in order to fulfil the requirement for using the optimal control derivation presented in the previous chapter i.e. the $\theta^* = 0$ should correspond to the $\text{mod}(t, 2\pi) = 0$. After shifting is done, the equations for the entrained solution as shown in (4.2) are implemented and solved using numerical ordinary differential equations method; these equations utilize the operational IRC and PRC obtained previously.

The shifted PRC and IRC are then utilized for computing the optimal control input according to the process highlighted in chapter 4. As an initial step, the operational PRC and IRC need to be converted back to the standard ones because the standard response curves are used for computing the optimal control input before going through the steps highlighted in section 4.3. In order to assess the usefulness and accuracy of the optimal control inputs obtained, the inputs (20 in total in this case) are then applied to the first component of the non-radial isochron model along with the entraining stimulus. Using the procedure detailed in the previous chapter, the standard controlled solution (4.1) containing both the optimal control input as well as entraining stimulus and the entrained solution (4.2), incorporating just the entraining stimulus, are calculated. From both the solutions mentioned before, phase and isostable coordinates are computed at k crossings of the initially defined threshold using

$$\begin{aligned}\psi_{cross} &= W(x(t) - x^{\gamma})e^{-\kappa t},\\ \theta_{cross} &= mod(\frac{2\pi(T-t)}{T}, 2\pi),\\ \theta^{*} &= \theta_{cross} + \frac{\alpha\psi_{cross}}{\kappa},\end{aligned} \tag{5.8}$$

where x^{γ} is the intial threshold defined for computing the phase-amplitude coordinates and W represents the left eigen vectors. Through (5.8), ψ_{cross}, θ_{cross} and θ^{*} are calculated and the values at the fourth or fifth crossing are considered. Note that as the phase response curve and the isostable response curve obtained through the adjoint method were scaled before, the left eigen vectors W have to be scaled accordingly in order to get accurate coordinates. Then, the difference between the phase-amplitude coordinates from the full/ standard controlled solution utilizing the optimal inputs and the phase-amplitude coordinates extracted through the entrained solution is taken.

The final section in this chapter describes the application of these obtained optimal control inputs in more detail and showcases the results from the non-radial isochron clock model by depicting the obtained PRC and IRC, the optimal control inputs and finally the effect on the recovery times when a time shift is applied to the model.

5.3 Illustration through the Non-radial Isochron Clock Model

Here, the proposed optimal control strategy is illustrated on the nonradial isochron clock model from (3.1):

$$\begin{aligned}\dot{x} &= \frac{2\pi}{T}\left[\sigma x(1-x^2-y^2) - y(1+\rho(x^2+y^2-1))\right] + f_e(t+h(T_e)\Delta t) + u(t) + \sqrt{2D}\eta(t),\\ \dot{y} &= \frac{2\pi}{T}\left[\sigma y(1-x^2-y^2) + x(1+\rho(x^2+y^2-1))\right].\end{aligned} \tag{5.9}$$

Equation (5.9) is identical to (3.1) except for the addition of the control input $u(t)$ and an independent and identically distributed, zero-mean white noise process $\sqrt{2D}\eta(t)$ with intensity D. As in Equation (3.1), the entraining stimulus is taken to be $f_e(t) = 0.025\sin(2\pi t/24 + 0.58)$. In this example, the term $h(T_e)$ is the unit step function that switches at time T_e and is used to model sudden time shifts in the light-dark cycle to mimic rapid travel across Δt time zones. All other constants and functions of (5.9) are taken to be the same as those from (3.1). For the moment, the noise strength is taken as $D = 0$ (the influence of noise will be considered momentarily). As demonstrated in Figure 3.2, the time required for reentrainment is directly related to the isostable (amplitude) coordinate directly before the external time shift. By implementing the control strategies from the previous chapter, it is possible to hasten recovery by applying a control designed to appropriately shift the isostable coordinate.

Towards obtaining the model dynamics in terms of phase and isostable coordinates, for the moment taking $f_e(t) = u(t) = 0$, the resulting periodic orbit has a period of $T = 24.2$ hours with a single nonunity Floquet multiplier $\lambda_1 = 0.605$ with corresponding Floquet exponent $\kappa_1 = -0.021$. The adjoint method [75], [7] is used to compute the asymptotic phase and isostable response curves for the transformation to phase and isostable coordinates (2.9) and (2.10) as discussed in the previous two sections. In this example, the input $u(t)$ is chosen to be the adjustable parameter with $u(t) = 0$ being the nominal value. When considering operational phase and isostable coordinates of this system, the $\theta^* = 0$ level set is defined to correspond to when $x(t)$ crosses 0 with a positive slope. With this definition of $\theta^* = 0$, $\alpha_1 = -0.0014$, computed according to Equation (2.14) indicating that increasing the isostable coordinate will slow down the nominal rate of oscillation. The subsequent operational phase response curves are computed from the asymptotic response curves using the relations given in (2.13). Figure 5.1 shows the corresponding operational and asymptotic phase and isostable response curves.

For the periodic orbit that results when $f_e(t) = 0$ in (5.9), solid lines in the left and right panels of Fig 5.1 show the asymptotic phase and isostable response curves, respectively, associated with input $u(t)$. Corresponding operational phase and isostable response curves are plotted with dashed lines. Note that $i_1(\theta)$ and $i_1^*(\theta^*)$ are identical.

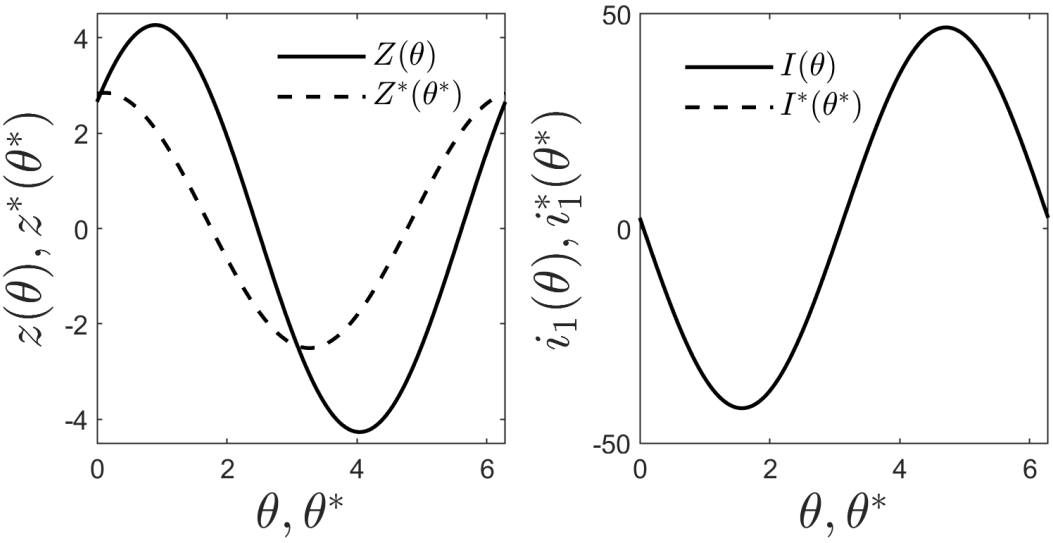

Figure 5.1: Standard and operational IRC and PRC for the non-radial isochron model [1]

The resulting operational phase and isostable reduced coordinate framework is used in conjunction with the optimal control strategy from the previous chapter. The calculus of variations approach is applied to minimize the cost functional (4.7) with resulting optimal inputs shown as solid lines in the left panel of Figure 5.2 for various values of X and negative values of Δt. Each input is designed to begin when $\text{mod}(t, 24) = 0$ for an initial condition that is fully entrained to the external input $f_e(t)$ and end 24 hours later, i.e., before a time shift at $T_e = 24$ hours.

Note that the fully entrained orbit has a period of 24 hours which is slightly faster than the period of the unperturbed orbit. Minimizing the cost functional from (4.7) balances the trade-off between maximizing the latent phase shift (to hasten recovery from a shift in external time) and minimizing the L^2 norm of the applied input. Smaller values of the weighting term X penalize the L^2 norm less thereby yielding larger magnitude inputs that give a larger latent phase. The approximate control input that minimizes the cost functional (4.33) is also shown using dashed lines of corresponding color. The resulting approximate optimal inputs and the inputs obtained from the solution of the Euler-Lagrange equations are nearly identical. Resulting optimal inputs are applied to the full model equations (5.9) in order to assess their effectiveness. Starting from a fully entrained solution at $t = 0$, inputs are applied on the interval $t = [0, 24]$ and the resulting isostable and operational phase coordinates are compared to $\theta_e^*(24)$ and $\psi_e(24)$, i.e., the values on the entrained solution; resulting differences are shown in the right panel of Figure 5.2. For values of X near 1, the resulting optimal inputs yield values of $\Delta\theta^*$ that are close to zero as desired. For large magnitude inputs that result when taking smaller values of X, the validity of the operational reduction starts to degrade due to nonlinear terms that are unaccounted for in the equations for the phase and isostable dynamics. This subsequently yields larger (undesired) shifts in the value of $\Delta\theta^*$. As such, only inputs that yield results with $|\Delta\psi| < 10$ will be considered further.

The optimal control strategy is designed to shift the isostable coordinates while leaving the operational phase coordinates unchanged. When considering the nonradial isochron clock model from (5.9), optimal control inputs that minimize the cost functional (4.7) using negative values of Δt are obtained using the calculus of variations approach (solid lines) and

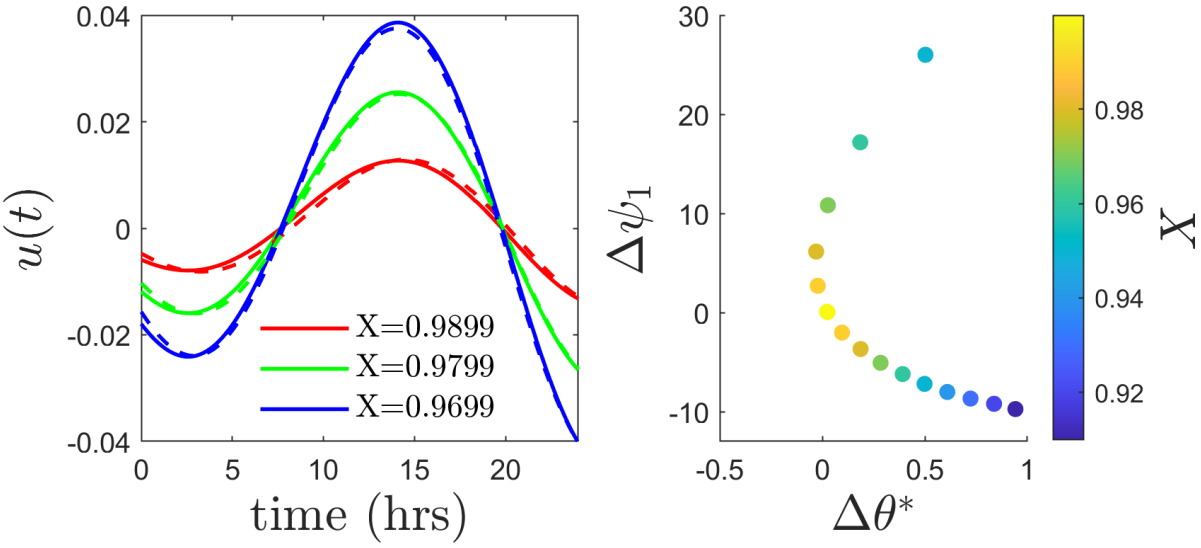

Figure 5.2: Obtained optimal control inputs and the corresponding phase amplitude shifts [1]

shown in the left panel for various choices of X in Fig 5.2. Approximations of the optimal inputs computed according to Equation (4.33) are shown as dashed lines. The right panel shows resulting values of $\Delta\psi_1$ and $\Delta\theta^*$ when optimal inputs obtained for both positive and negative values of Δt are applied to the full model equations (5.9). The dashed red line shows the target value of $\Delta\theta = 0$. The proposed method yields results that are close to this target value when the input magnitudes are small. This effectiveness is degraded for smaller values of X which yield larger magnitude inputs.

Finally, the recovery times of the resulting optimal stimuli are investigated with results shown in Figure 5.3. In order to measure the recovery times following a given time shift, the system (5.9) is first simulated with $u(t) = 0$ until it is fully entrained to $f_e(t)$. At this point, for a given choice of X where X ranges from 0.9999 to 0.9099 with 0.01 decrements, the corresponding optimal stimulus is applied over a 24-hour period to produce an associated shift in the isostable coordinate $\Delta\psi_1$. Immediately after the conclusion of the application of the optimal stimulus, at $T_e = 24$ hours the external time is shifted by some amount Δt, representing rapid travel through multiple time zones. The subsequent recovery time is taken to be the amount of time required for θ^* to return to within one hour of the fully entrained solution. The right panel of Figure 5.3 shows the resulting recovery times. For the curve corresponding to $\Delta\psi_1 = 0$, i.e., that results when $u(t) = 0$, there is a two hour window centered at $\Delta t = 0$ within which the recovery time is zero since, by definition, the time shift is so small that recovery happens immediately. By applying an optimal input before the external time shift occurs, this window is shifted in response to the shifted isostable coordinate. Positive (resp., negative) shifts in the isostable coordinate yield more rapid recoveries for negative (resp., positive) shifts in time. The left panel of Figure 5.3 shows the recovery in response to a time shift of $\Delta t = +5$ hours illustrating that by first applying a stimulus that yields a decrease in the isostable coordinate, subsequent recovery is hastened.

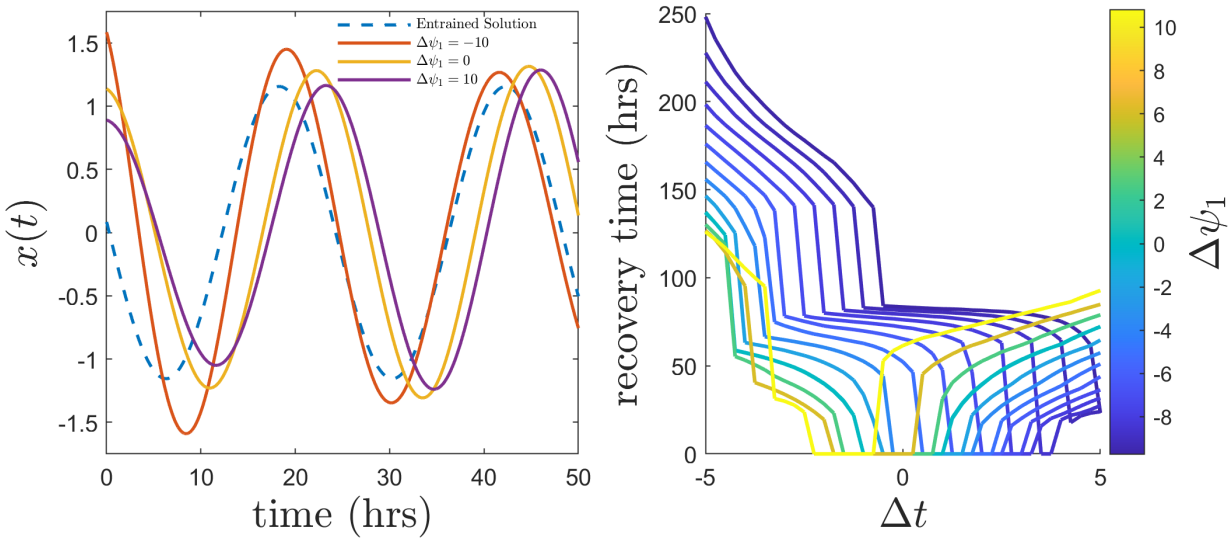

Figure 5.3: Recovery times from different shifts in time based upon the shift in isostable coordinates [1]

Chapter 6

Conclusion

In this work, the influence of circadian memory was investigated in the context of recovery from circadian misalignment. An operational phase and isostable reduced order modeling framework was used to capture the behavior of slowly decaying amplitude coordinates that depend on the past input history. By analyzing the operational phase and isostable reduced equations, a latent phase shift was identified (highlighted in (4.8)) that is directly proportional to the isostable coordinates and can be used to prime the underlying system to recover more rapidly to an expected shift in the environmental time. A subsequent optimal control formulation is proposed that balances the trade-off between control effort and the resulting latent phase shift. Explicit, approximate solutions for this optimal control problem are also derived that are valid in the limit that the magnitude of the input is small. Finally, the resulting control strategy is validated on a simple model (5.9) that exhibits entrained oscillations

The proposed control strategy to hasten recovery from circadian misalignment differs from previously considered control frameworks in its explicit consideration of memory effects. In contrast, many previously considered control strategies (e.g., [4], [80], [17], [55]) seek to find inputs that will hasten realignment in response to a time shift when starting from a nominally fully entrained state. Other pretreatment strategies [52], [16], [9] have been proposed to shift the nominal phase prior to expected travel across multiple time zones, but do not consider amplitude-based effects. The proposed strategy is designed to modify the amplitude coordinates associated with a nominally entrained oscillation *without changing the*

phase prior to the expected time shift; here, the associated latent phase shift influences the subsequent recovery. In this work, in order to isolate the influence of the isostable coordinates on the recovery from circadian misalignment, optimal solutions of the cost functional (4.7) are required to satisfy $\Delta\theta^*(T_e) = 0$, that is, optimal inputs are not allowed to modify θ^*. It would be of interest in future work to consider solutions for which $\Delta\theta^*(T_e)$ could take nonzero values. This would certainly allow for faster recovery from circadian misalignment by both shifting the operational phase and the latent phase appropriately.

There are many limitations that the work in this thesis does not directly consider. Foremost, the model used to represent coupled circadian oscillations does not accurately capture the complicated physiologically relevant processes governing circadian rhythms. More detailed models of gene regulation such as [49], [31], [36], [42] would be necessary to investigate the influence of circadian memory on recovery from circadian misalignment. Additionally, the operational phase and isostable reduced order models used in this work are only valid to first order accuracy in the amplitude coordinates. As such the resulting optimal control inputs are required to be sufficiently small so that the validity of the reduced order model is not degraded. It would also be of interest to extend this control framework for phase-isostable-based models that are valid to higher orders of accuracy such as those from [67] or [66]. These and other practical considerations can potentially be investigated in future work.

Bibliography

[1] Ahmed, T. and Wilson, D. (2021). Exploiting circadian memory to hasten recovery from circadian misalignment. *Chaos: An Interdisciplinary Journal of Nonlinear Science*, 31(7):073130. iv, vii, 18, 35, 37, 39

[2] An, S., Harang, R., Meeker, K., Granados-Fuentes, D., Tsai, C. A., Mazuski, C., Kim, J., Doyle, F. J., Petzold, L. R., and Herzog, E. D. (2013). A neuropeptide speeds circadian entrainment by reducing intercellular synchrony. *Proceedings of the National Academy of Sciences*, 110(46):E4355–E4361. 3

[3] Arendt, J. (2009). Managing jet lag: some of the problems and possible new solutions. *Sleep Medicine Reviews*, 13(4):249–256. 1

[4] Bagheri, N., Stelling, J., and III, F. J. D. (2008). Circadian phase resetting via single and multiple control targets. *PLoS Computational Biology*, 4(7):e1000104. 2, 40

[5] Beaumont, M., Batejat, D., Pierard, C., Beers, P. V., Denis, J. B., Coste, O., Doireau, P., Chauffard, F., French, J., and Lagarde, D. (2004). Caffeine or melatonin effects on sleep and sleepiness after rapid eastward transmeridian travel. *Journal of Applied Physiology*, 96(1):50–58. 2

[6] Bedrosian, T. and Nelson, R. (2017). Timing of light exposure affects mood and brain circuits. *Translational psychiatry*, 7(1):e1017–e1017. 2

[7] Brown, E., Moehlis, J., and Holmes, P. (2004). On the phase reduction and response dynamics of neural oscillator populations. *Neural Computation*, 16(4):673–715. 11, 34

[8] Brown, S. A., Fleury-Olela, F., Nagoshi, E., Hauser, C., Juge, C., Meier, C. A., Chicheportiche, R., Dayer, J. M., Albrecht, U., and Schibler, U. (2005). The period length of fibroblast circadian gene expression varies widely among human individuals. *PLoS Biology*, 3(10):e338. 16

[9] Burgess, H. J., Crowley, S. J., Gazda, C. J., Fogg, L. F., and Eastman, C. I. (2003). Preflight adjustment to eastward travel: 3 days of advancing sleep with and without morning bright light. *Journal of Biological Rhythms*, 18(4):318–328. 2, 3, 40

[10] Burgess, H. J., Revell, V. L., and Eastman, C. I. (2008). A three pulse phase response curve to three milligrams of melatonin in humans. *The Journal of Physiology*, 586(2):639–647. 2

[11] Chesson, A. L., Littner, M., Davila, D., Anderson, W. M., Grigg-Damberger, M., Hartse, K., Johnson, S., and Wise, M. (1999). Practice parameters for the use of light therapy in the treatment of sleep disorders. *Sleep*, 22(5):641–660. 2

[12] Cho, K., Ennaceur, A., Cole, J. C., and Suh, C. K. (2000). Chronic jet lag produces cognitive deficits. *Journal of Neuroscience*, 20(6):RC66–RC66. 2

[13] Czeisler, C. A., Duffy, J. F., Shanahan, T. L., Brown, E. N., Mitchell, J. F., Rimmer, D. W., Ronda, J. M., Silva, E. J., Allan, J. S., Emens, J. S., et al. (1999). Stability, precision, and near-24-hour period of the human circadian pacemaker. *Science*, 284(5423):2177–2181. 16

[14] Davidson, A. J., Sellix, M. T., Daniel, J., Yamazaki, S., Menaker, M., and Block, G. D. (2006). Chronic jet-lag increases mortality in aged mice. *Current Biology*, 16(21):R914–R916. 2

[15] Daymude, J. A. and Refinetti, R. (1999). Phase-shifting effects of single and multiple light pulses in the golden hamster. *Biological Rhythm Research*, 30(2):202–215. 2

[16] Deacon, S. and Arendt, J. (1996). Adapting to phase shifts, I. an experimental model for jet lag and shift work. *Physiology & behavior*, 59(4-5):665–673. 2, 3, 40

[17] Dean, D. A., Forger, D. B., and Klerman, E. B. (2009). Taking the lag out of jet lag through model-based schedule design. *PLoS Comput Biol*, 5(6):e1000418. 2, 6, 40

[18] Diekman, C. O. and Bose, A. (2018). Reentrainment of the circadian pacemaker during jet lag: east-west asymmetry and the effects of north-south travel. *Journal of Theoretical Biology*, 437:261–285. 5

[19] Eastman, C. I. and Burgess, H. J. (2009). How to travel the world without jet lag. *Sleep Medicine Clinics*, 4(2):241–255. 6

[20] Filipski, E., Delaunay, F., King, V. M., Wu, M. W., Claustrat, B., Gréchez-Cassiau, A., Guettier, C., Hastings, M. H., and Francis, L. (2004). Effects of chronic jet lag on tumor progression in mice. *Cancer Research*, 64(21):7879–7885. 2

[21] Filipski, E., Subramanian, P., Carriere, J., Guettier, C., Barbason, H., and Levi, F. (2009). Circadian disruption accelerates liver carcinogenesis in mice. *Mutation Research/Genetic Toxicology and Environmental Mutagenesis*, 680(1):95–105. 2

[22] Golombek, D. A. and Rosenstein, R. E. (2010). Physiology of circadian entrainment. *Physiological Reviews*, 90(3):1063–1102. 1

[23] Guckenheimer, J. (1975). Isochrons and phaseless sets. *Journal of Mathematical Biology*, 1(3):259–273. 7, 8

[24] Haimov, I. and Arendt, J. (1999). The prevention and treatment of jet lag. *Sleep Medicine Reviews*, 3(3):229–240. 2

[25] Harada, T., Tanaka, H. A., Hankins, M. J., and Kiss, I. Z. (2010). Optimal waveform for the entrainment of a weakly forced oscillator. *Physical Review Letters*, 105(8):088301. 2

[26] Hastings, M. H. and Goedert, M. (2013). Circadian clocks and neurodegenerative diseases: time to aggregate? *Current opinion in neurobiology*, 23(5):880–887. vii, 4

[27] Hébert, M., Martin, S. K., Lee, C., and Eastman, C. I. (2002). The effects of prior light history on the suppression of melatonin by light in humans. *Journal of Pineal Research*, 33(4):198–203. 2

[28] Jordan, D. and Smith, P. (2007). *Nonlinear ordinary differential equations: an introduction for scientists and engineers*, volume 10. Oxford University Press, Oxford. 8

[29] Jr, N. C. R. and Montgomery, R. (2002). Using the Argonne diet in jet lag prevention: deployment of troops across nine time zones. *Military Medicine*, 167(6):451–453. 6

[30] Khalsa, S. B. S., Jewett, M. E., Cajochen, C., and Czeisler, C. A. (2003). A phase response curve to single bright light pulses in human subjects. *The Journal of Physiology*, 549(3):945–952. 2

[31] Kim, J. K. and Forger, D. B. (2012). A mechanism for robust circadian timekeeping via stoichiometric balance. *Molecular Systems Biology*, 8(1):630. 41

[32] Kirk, D. (1998). *Optimal Control Theory*. Dover Publications, New York. 23, 24, 27

[33] Kott, J., Leach, G., and Yan, L. (2012). Direction-dependent effects of chronic "jet-lag" on hippocampal neurogenesis. *Neuroscience Letters*, 515(2):177–180. 2

[34] Kuramoto, Y. (1984). *Chemical Oscillations, Waves, and Turbulence*. Springer-Verlag, Berlin. 7

[35] Kvalheim, M. D. and Revzen, S. (2019). Existence and uniqueness of global Koopman eigenfunctions for stable fixed points and periodic orbits. *arXiv preprint 1911.11996*. 10

[36] Leloup, J. C. and Goldbeter, A. (2003). Toward a detailed computational model for the mammalian circadian clock. *Proceedings of the National Academy of Sciences*, 100(12):7051–7056. 41

[37] Leloup, J. C. and Goldbeter, A. (2013). Critical phase shifts slow down circadian clock recovery: implications for jet lag. *Journal of Theoretical Biology*, 333:47–57. 2, 6

[38] Lewy, A. J., Bauer, V. K., Ahmed, S., Thomas, K. H., Cutler, N. L., Singer, C. M., Moffit, M. T., and Sack, R. L. (1998). The human phase response curve (PRC) to melatonin is about 12 hours out of phase with the PRC to light. *Chronobiology International*, 15(1):71–83. 2

[39] Lu, Z., Klein-Cardeña, K., Lee, S., Antonsen, T. M., Girvan, M., and Ott, E. (2016). Resynchronization of circadian oscillators and the east-west asymmetry of jet-lag. *Chaos: An Interdisciplinary Journal of Nonlinear Science*, 26(9):094811. 7

[40] Mezić, I. (2019). Spectrum of the Koopman operator, spectral expansions in functional spaces, and state-space geometry. *Journal of Nonlinear Science*, pages 1–55. 10

[41] Minors, D. S., Waterhouse, J. M., and Wirz-Justice, A. (1991). A human phase-response curve to light. *Neuroscience Letters*, 133(1):36–40. 2

[42] Mirsky, H. P., Liu, A. C., Welsh, D. K., Kay, S. A., and Doyle, F. J. (2009). A model of the cell-autonomous mammalian circadian clock. *Proceedings of the National Academy of Sciences*, 106(27):11107–11112. 41

[43] Monga, B., Wilson, D., Matchen, T., and Moehlis, J. (2019). Phase reduction and phase-based optimal control for biological systems: a tutorial. *Biological Cybernetics*, 113(1-2):11–46. 6, 11, 29

[44] Moore, R. Y., Speh, J. C., and Leak, R. K. (2002). Suprachiasmatic nucleus organization. *Cell and Tissue Research*, 309(1):89–98. 1

[45] Panda, S., Hogenesch, J. B., and Kay, S. A. (2002). Circadian rhythms from flies to human. *Nature*, 417(6886):329. 1

[46] Piérard, C., Beaumont, M., Enslen, M., Chauffard, F., Tan, D. X., Reiter, R. J., Fontan, A., French, J., Coste, O., and Lagarde, D. (2001). Resynchronization of hormonal rhythms after an eastbound flight in humans: effects of slow-release caffeine and melatonin. *European Journal of Applied Physiology*, 85(1-2):144–150. 2

[47] Pyragas, K., Fedaravičius, A. P., Pyragienė, T., and Tass, P. A. (2018). Optimal waveform for entrainment of a spiking neuron with minimum stimulating charge. *Physical Review E*, 98(4):042216. 2

[48] Refinetti, R. (2002). Compression and expansion of circadian rhythm in mice under long and short photoperiods. *Integrative Physiological & Behavioral Science*, 37(2):114–127. 2

[49] Relógio, A., Westermark, P. O., Wallach, T., Schellenberg, K., Kramer, A., and Herzel, H. (2011). Tuning the mammalian circadian clock: robust synergy of two loops. *PLoS Computational Biology*, 7(12):e1002309. 41

[50] Reppert, S. M. and Weaver, D. R. (2002). Coordination of circadian timing in mammals. *Nature*, 418(6901):935. 1

[51] Revell, V. L., Burgess, H. J., Gazda, C. J., Smith, M. R., Fogg, L. F., and Eastman, C. I. (2006). Advancing human circadian rhythms with afternoon melatonin and morning intermittent bright light. *The Journal of Clinical Endocrinology & Metabolism*, 91(1):54–59. 2

[52] Revell, V. L. and Eastman, C. I. (2005). How to trick mother nature into letting you fly around or stay up all night. *Journal of Biological Rhythms*, 20(4):353–365. 2, 3, 40

[53] Sack, R. L. (2010). Jet lag. *New England Journal of Medicine*, 362(5):440–447. 1, 2

[54] Samuels, C. H. (2012). Jet lag and travel fatigue: a comprehensive management plan for sport medicine physicians and high-performance support teams. *Clinical Journal of Sport Medicine*, 22(3):268–273. 2

[55] Serkh, K. and Forger, D. B. (2014). Optimal schedules of light exposure for rapidly correcting circadian misalignment. *PLoS Computational Biology*, 10(4):e1003523. 2, 40

[56] Shimomura, K. and Menaker, M. (1994). Light-induced phase shifts in tau mutant hamsters. *Journal of Biological Rhythms*, 9(2):97–110. 2

[57] Shirasaka, S., Kurebayashi, W., and Nakao, H. (2017). Phase-amplitude reduction of transient dynamics far from attractors for limit-cycling systems. *Chaos: An Interdisciplinary Journal of Nonlinear Science*, 27(2):023119. 8

[58] Suhner, A., P.Schlagenhauf, Johnson, R., Tschopp, A., and Steffen, R. (1998). Comparative study to determine the optimal melatonin dosage form for the alleviation of jet lag. *Chronobiology International*, 15(6):655–666. 2

[59] Taylor, S. R., Gunawan, R., Petzold, L. R., and III, F. J. D. (2008). Sensitivity measures for oscillating systems: Application to mammalian circadian gene network. *IEEE Transactions on Automatic Control*, 53:177–188. 2, 7

[60] Vaccaro, A., Birman, S., and Klarsfeld, A. (2016). Chronic jet lag impairs startle-induced locomotion in drosophila. *Experimental Gerontology*, 85:24–27. 2

[61] vanderLeest, H. T., Rohling, J. H. T., Michel, S., and Meijer, J. H. (2009). Phase shifting capacity of the circadian pacemaker determined by the scn neuronal network organization. *PLoS One*, 4(3):e4976. 2

[62] Vosko, A. M., Colwel, C. S., and Avidan, A. Y. (2010). Jet lag syndrome: circadian organization, pathophysiology, and management strategies. *Nature and Science of Sleep*, 2:187. 6

[63] Waterhouse, J., Reilly, T., Atkinson, G., and Edwards, B. (2007). Jet lag: trends and coping strategies. *The Lancet*, 369(9567):1117–1129. 2

[64] Wiggins, S. (2003). *Introduction to applied nonlinear dynamical systems and chaos*, volume 2. Springer. 13

[65] Wilson, D. (2019). Isostable reduction of oscillators with piecewise smooth dynamics and complex floquet multipliers. *Physical Review E*, 99(2):022210. 11

[66] Wilson, D. (2020a). An adaptive phase-amplitude reduction framework without $\mathcal{O}(\epsilon)$ constraints on inputs. *arXiv preprint 2011.10410*. 41

[67] Wilson, D. (2020b). Phase-amplitude reduction far beyond the weakly perturbed paradigm. *Physical Review E*, 101(2):022220. 11, 41

[68] Wilson, D. and Ermentrout, B. (2018a). Greater accuracy and broadened applicability of phase reduction using isostable coordinates. *Journal of Mathematical Biology*, 76(1-2):37–66. 8, 11

[69] Wilson, D. and Ermentrout, B. (2018b). An operational definition of phase characterizes the transient response of perturbed limit cycle oscillators. *SIAM Journal on Applied Dynamical Systems*, 17(4):2516–2543. vii, 3, 5, 8, 13, 14, 15

[70] Wilson, D. and Ermentrout, B. (2019). Augmented phase reduction of (not so) weakly perturbed coupled oscillators. *SIAM Review*, 61(2):277–315. 11, 21

[71] Wilson, D., Holt, A. B., Netoff, T. I., and Moehlis, J. (2015). Optimal entrainment of heterogeneous noisy neurons. *Frontiers in Neuroscience*, 9:192. 2

[72] Wilson, D. and Moehlis, J. (2014a). An energy-optimal approach for entrainment of uncertain circadian oscillators. *Biophysical Journal*, 107(7):1744–1755. 2

[73] Wilson, D. and Moehlis, J. (2014b). Optimal chaotic desynchronization for neural populations. *SIAM Journal on Applied Dynamical Systems*, 13(1):276–305. vii, 9

[74] Wilson, D. and Moehlis, J. (2015). Extending phase reduction to excitable media: theory and applications. *siam REVIEW*, 57(2):201–222. vii, 12

[75] Wilson, D. and Moehlis, J. (2016). Isostable reduction of periodic orbits. *Physical Review E*, 94(5):052213. 8, 11, 34

[76] Winfree, A. (2001). *The Geometry of Biological Time*. Springer Verlag, New York, second edition. 7, 8, 16

[77] Wright, K. P., Hughes, R. J., Kronauer, R. E., Dijk, D. J., and Czeisler, C. A. (2001). Intrinsic near-24-h pacemaker period determines limits of circadian entrainment to a weak synchronizer in humans. *Proceedings of the National Academy of Sciences*, 98(24):14027–14032. 1

[78] Yamaguchi, Y., Suzuki, T., Mizoro, Y., Kori, H., Okada, K., Chen, Y., Fustin, J. M., Yamazaki, F., Mizuguchi, N., Zhang, J., Dong, X., Tsujimoto, G., Okuno, Y., Doi, M., and Okamura, H. (2013). Mice genetically deficient in vasopressin V1a and V1b receptors are resistant to jet lag. *Science*, 342(6154):85–90. 3, 6

[79] Young, M. W. and Kay, S. A. (2001). Time zones: a comparative genetics of circadian clocks. *Nature Reviews Genetics*, 2(9):702. 1

[80] Zhang, J., Bierman, A., Wen, J. T., Julius, A., and Figueiro, M. (2010). Circadian system modeling and phase control. In *2010 49th IEEE Conference on Decision and Control*, pages 6058–6063. IEEE. 2, 40

[81] Zlotnik, A., Chen, Y., Kiss, I. Z., Tanaka, H. A., and Li, J. S. (2013). Optimal waveform for fast entrainment of weakly forced nonlinear oscillators. *Physical Review Letters*, 111(2):024102. 2

Appendix

A Detailed Derivation for the Presented Optimal Control Strategy

This Appendix provides the step by step details regarding how exactly the optimal control methodology was derived.

A.1 Approximate Optimal Control Derivation for Multiple Isostable Coordinates

First of all, for the derivation, the Cost functional needs to be defined. Recall that the operational phase and isostable coordinates are given by

$$\begin{aligned}\dot{\theta^*} &= \omega + \sum_{j=1}^{\beta}(\alpha_j\psi_j) + Z^*(\theta^*)^T u(t),\\ \dot{\psi_i} &= \kappa_i\psi_i + I_i^*(\theta^*)^T u(t),\\ i &= 1,\ldots,\beta. \end{aligned} \tag{1}$$

where β represents the total number of isostable coordinates. Now, it is known that the relationship between standard and operational phase can be defined according to

$$\theta = \theta^* - \frac{\alpha_j\psi_j}{\kappa_j}, \tag{2}$$

If the input $u(t)$ is taken to be zero in (1), the resulting equations are:

$$\begin{aligned}\dot{\theta^*} &= \omega + \sum_{j=1}^{N-1}(\alpha_j\psi_j),\\ \psi_i(t) &= \psi_i(0)exp(\kappa_i t). \end{aligned} \tag{3}$$

Using (2), the latent phase difference between the standard and operational phase can be written as

$$\sum_{i=1}^{\beta} \int_0^{\infty} \psi_i(0) exp(\kappa_i t) dt = \sum_{i=1}^{\beta} -\frac{\alpha_j \psi_j(0)}{\kappa_j}, \tag{4}$$

And finally, using (4), the cost functional can be written as

$$C = \int_0^T X u^2(t) dt + (1 - X) \sum_{i=1}^{\beta} (-\frac{\alpha_j \psi_j(T)}{\kappa_j}), \tag{5}$$

where X $\in [0, 1]$ is defined as the weighting coeffiecient in the cost functional. Furthermore, considering (1), assume $u(t) = O(\epsilon)$ where $0 < \epsilon \ll 1$ and then the operational phase can be written as

$$\dot{\theta}^* = \omega + O(\epsilon), \tag{6}$$

which can be integrated to

$$\theta^* = \theta^*(0) + \omega t, \tag{7}$$

If the state is said to be on periodic orbit, then $\theta^*(0) = 0$ and $\psi_i(0) = 0$ and moreover, let $= \psi_i(t) e^{-\kappa_i t}$. The isostable coordinate equation from (1) can be rewritten as

$$\dot{\psi}_i = \dot{r}_i e^{\kappa_i t} + \kappa_i r_i e^{\kappa_i t} = \kappa_i r_i e^{\kappa_i t} + I_i(\omega t) u(t), \tag{8}$$

which can be rearranged and integrated to get

$$\begin{aligned} \dot{r}_i &= e^{-\kappa_i t} I_i(\omega t) u(t), \\ r_i(t) &= r(t_0) + \int_0^t e^{-\kappa s} I_i(\omega s) u(s) ds. \end{aligned} \tag{9}$$

Substituting $\psi_i = r_i e^{\kappa_i t}$ into the equation above and utilizing the assumption that $\psi_i(0) = 0$ finally yields

$$\psi_i(T) = \int_{t_0=0}^{T} e^{\kappa_i (T-s)} I_i(\omega s) u(s) ds, \tag{10}$$

By writing the isotable coordinates in the form depicted in (10), the dimensionality of the resulting reduced order model framework can be greatly reduced as the dynamical equations

governing each individual isostable coordinate ψ_i can be eliminated entirely. Furthermore, if (10) is utilized in the cost functional in (5), one can get

$$C = \int_0^T \left[Xu^2(s) + (1-X) \sum_{j=1}^{\beta} -\frac{\alpha_j}{\kappa_j} e^{\kappa_j (T-s)} I_j(\omega s) u(s) \right] ds, \tag{11}$$

Another constraint, that needs to be incorporated into the derivation, is $\theta^*(T) = 0$. For achieving that, it is known that

$$\theta^* = \theta + \sum_{i=1}^{\beta} \frac{\alpha_j \psi_j}{\kappa_j}, \tag{12}$$

Now, θ is equivalent to $\int_0^T Z(\omega t) u(t) dt$ to leading order ϵ; the ψ_i is already known from (10). So, the final constraint equation can be written as

$$0 = \int_0^T \left[Z(\omega s) u(s) + \sum_{j=1}^{\beta} -\frac{\alpha_j}{\kappa_j} e^{\kappa_j (T-s)} I_j(\omega s) u(s) \right] ds, \tag{13}$$

(13) can be written as an ordinary differential equation with $P_1(0) = P_1(T) = 0$ as:

$$\frac{d}{ds} P_1 = Z(\omega s) u(s) + \sum_{j=1}^{\beta} -\frac{\alpha_j}{\kappa_j} e^{\kappa_j (T-s)} I_j(\omega s) u(s), \tag{14}$$

In order to find the optimal control input $u(t)$, the cost functional as well as the constraint equation in (11) and (13) respectively can be combined as shown below in order to find the function M that needs to be minimized by $u(t)$

$$\begin{aligned} M = \int_0^T & Xu^2(s) + (1-X) \sum_{j=1}^{\beta} -\frac{\alpha_j}{\kappa_j} e^{\kappa_j (T-s)} I_j(\omega s) u(s) \\ & + \lambda_1 \left[Z(\omega s) u(s) + \sum_{j=1}^{\beta} -\frac{\alpha_j}{\kappa_j} e^{\kappa_j (T-s)} I_j(\omega s) u(s) - \dot{P}_1 \right] ds, \end{aligned} \tag{15}$$

where λ_1 is the lagrange multiplier for positive isostable coordinates. The integrand of function M is denoted by γ and is used for deriving the Euler Lagrange equations. Through the Euler Lagrange equations, the optimal control input $u(s)$ is found by using $\frac{\delta \gamma}{\delta u} = \frac{d}{ds} \left(\frac{\delta \gamma}{\delta \dot{u}} \right)$

as:

$$u(s) = \left(\frac{-1}{2}\right)\left(\frac{\alpha}{\kappa}\right)e^{\kappa(T-t)}I(\omega s) + \left(\frac{-1}{2X}\right)\lambda_1 Z(\omega s) + \left(\frac{-1}{2X}\right)(\lambda_1 - 1)\left(\frac{\alpha}{\kappa}\right)e^{\kappa(T-t)}I(\omega s)), \quad (16)$$

Similarly, through $\frac{\delta\gamma}{\delta P_1} = \frac{d}{ds}\left(\frac{\delta\gamma}{\delta \dot{P}_1}\right)$, it can be found that $\frac{d}{ds}\lambda_1 = 0$ which clearly indicates that λ_1 is a constant. Finally, the value of λ_1 is found by substituting (16) in (13) and the resulting equations are

$$\begin{aligned}
eq1 = &-\left(\frac{1}{2X}\right)Z^2(\omega s) - \left(\frac{Z(\omega s)}{2X}\right)\left(\frac{\alpha}{\kappa}\right)e^{\kappa(T-t)}I(\omega s) \\
&- \left(\frac{Z(\omega s)}{2X}\right)\left(\frac{\alpha}{\kappa}\right)e^{\kappa(T-t)}I(\omega s) - \left(\frac{1}{2X}\right)\left(\left(\frac{\alpha}{\kappa}\right)e^{\kappa(T-t)}I(\omega s)\right)^2, \\
eq2 = &\left(\frac{Z(\omega s)}{2X}\right)\left(\frac{\alpha}{\kappa}\right)e^{\kappa(T-t)}I(\omega s) + \left(\frac{1}{2X}\right)\left(\left(\frac{\alpha}{\kappa}\right)e^{\kappa(T-t)}I(\omega s)\right)^2 \\
&- \left(\frac{Z(\omega s)}{2}\right)\left(\frac{\alpha}{\kappa}\right)e^{\kappa(T-t)}I(\omega s) - \left(\frac{1}{2}\right) * \left(\left(\frac{\alpha}{\kappa}\right)e^{\kappa(T-t)}I(\omega s)\right)^2. \qquad (17)
\end{aligned}$$

Using numerical integration, the equations above can be utilized in order to get the initial value of lambda which can then be used in (16) to get the optimal control input. It is to be noted that the same control derivation can be extended to negative isostable coordinates by changing the sign in (4). The relevant optimal control input equation is given by

$$u(s) = \left(\frac{1}{2}\right)\left(\frac{\alpha}{\kappa}\right)e^{\kappa(T-t)}I(\omega s) + \left(\frac{-1}{2X}\right)\lambda_2 Z(\omega s) - \left(\frac{1}{2X}\right)(\lambda_2 + 1)\left(\frac{\alpha}{\kappa}\right)e^{\kappa(T-t)}I(\omega s)), \quad (18)$$

and equations for finding λ_2 or the lagrange multiplier for negative isostable coordinates through numerical integration is

$$\begin{aligned}
eq3 = &\left(\frac{-1}{2X}\right)Z^2(\omega s) - \left(\frac{Z(\omega s)}{2X}\right)\left(\frac{\alpha}{\kappa}\right)e^{\kappa(T-t)}I(\omega s) \\
&- \left(\frac{Z(\omega s)}{2X}\right)\left(\frac{\alpha}{\kappa}\right)e^{\kappa(T-t)}I(\omega s) - \left(\frac{1}{2X}\right)\left(\left(\frac{\alpha}{\kappa}\right)e^{\kappa(T-t)}I(\omega s)\right)^2, \\
eq4 = &\left(\frac{-Z(\omega s)}{2X}\right)\left(\frac{\alpha}{\kappa}\right)e^{\kappa(T-t)}I(\omega s) - \left(\frac{1}{2X}\right)\left(\left(\frac{\alpha}{\kappa}\right)e^{\kappa(T-t)}I(\omega s)\right)^2 \\
&+ \left(\frac{Z(\omega s)}{2}\right)\left(\frac{\alpha}{\kappa}\right)e^{\kappa(T-t)}I(\omega s) + \left(\frac{1}{2}\right) * \left(\left(\frac{\alpha}{\kappa}\right)e^{\kappa(T-t)}I(\omega s)\right)^2. \qquad (19)
\end{aligned}$$

A.2 Revised Optimal Control Derivation for Multiple Isostable Coordinates

In the previous derivation in Appendix A.1, it was noted that $Z(\omega s)$ turns out to be equal to zero due to the presence of the entraining stimulus which, in turn, caused the optimal control input to turn to zero. In order to overcome this issue, some changes were made to the original derivation by rewriting the operational phase and isostable coordinates as shown below:

$$\begin{aligned}
\dot{\theta}^* &= \omega + \sum_{i=1}^{\beta}(\alpha_i\psi_i) + \epsilon Z^*(\theta^*)u(t) + \epsilon u_e(t)Z^*(\theta^*),\\
\dot{\psi}_i &= \kappa_i\psi_i + \epsilon I_i^*(\theta^*)u(t) + \epsilon I_i^*(\theta^*)u_e(t),\\
i &= 1,\ldots,\beta.
\end{aligned} \tag{20}$$

Equation (20) above divides the original optimal control input into control input and entraining stimulus input. It is assumed that each ψ_i, control and entraining stimulus are $O(\epsilon)$ terms; furthermore, the entraining stimulus u_e is periodic with time period T_e and $\omega_e = \frac{2\pi}{T_e}$. Similarly, the difference between the nominal and entrained angular frequency i.e. $\omega - \omega_e$ is of the order $O(\epsilon)$. On the other hand, the entrained reduced equations (i.e. when $u(t) = 0$) is defined by

$$\begin{aligned}
\dot{\theta_E^*} &= \omega + \sum_{i=1}^{\beta}(\alpha_i\psi_i) + \epsilon u_e(t)Z^*(\theta^*),\\
\dot{\psi}_{iE} &= \kappa_i\psi_i + \epsilon I_{iE}^*(\theta^*)u_e(t),
\end{aligned} \tag{21}$$

where $\theta_E^*(t)$ is the entrained solution and ψ_{iE} represents the associated isostable coordinates. Now, consider $\Delta\theta^* = \theta^* - \theta_E^*$ and $\Delta\psi_i = \psi_i - \psi_{iE}$ i.e. the difference between the controlled solution with $u(t) \neq 0$ and the entrained solution. The equation for $\Delta\dot{\theta}^*$ is given by

$$\Delta\dot{\theta}^* = \dot{\theta}^* - \dot{\theta}_E = \sum_{i=1}^{\beta}\alpha_i\Delta\psi_i + \epsilon Z^*(\theta^*)u(t) + \epsilon u_e(t)[Z^*(\theta^*) - Z(\theta_E^*)], \tag{22}$$

The term $\epsilon u_e(t)[Z^*(\theta^*) - Z(\theta_E^*)]$ is of the order $O(\epsilon^2)$ and hence can be ignored according to the $O(\epsilon)$ assumption made earlier. So, after simplification, one can get

$$\dot{\theta}^* = \sum_{i=1}^{\beta} \alpha_i \Delta\psi_i + \epsilon Z^*(\theta_0 + \omega_e t)u(t), \tag{23}$$

An important point to note here is that $Z^*(\theta_0 + \omega_e t)$ is obtained from the non-entrained limit cycle. Likewise, when considering $\Delta\dot{\psi}_i$, one gets $\epsilon[I_i(\theta^*) - I_i(\theta_E^*)]u(t)$ which is again of the order $O(\epsilon^2)$ and hence, can be ignored one again. The resulting equation for $\Delta\dot{\psi}_i$ is

$$\Delta\dot{\psi}_i = \kappa_i \Delta\psi_i + \epsilon I_i(\theta_0 + \omega_e t)u, \tag{24}$$

When $u(t) = 0$, equation (24) gets changed to $\Delta\dot{\psi}_i = \kappa_i \Delta\psi_i$ which means that the latent phase difference used in (4) can still be used in the cost functional as

$$C = \int_0^T X u^2(t) dt + (1 - X) \sum_{i=1}^{\beta} (-\frac{\alpha_j \Delta\psi_j(T)}{\kappa_j}), \tag{25}$$

The rest of the procedure for computing the optimal control input, including the constraint, is identical to the derivation presented in Appendix A.1 which means that the (16), (17), (18) and (19) can be utilized here as well with no major difference except now, the unentrained limit cycle is used for deriving the optimal control input. In order to make use of this derivation properly, some things to note are:

- $\theta = 0$ needs to be taken corresponding to $\text{mod}(t, 2\pi) = 0$.
- Instead of ω, ω_e is used in (23) and (24); this is still accurate as $\omega = \omega_e + O(\epsilon)$ which means that making this switch only causes an error of $O(\epsilon)$. However, the optimal control input must be derived considering the entrained time period T_e, not the free running/ unperturbed period.

Vita

Talha Ahmed is originally from Pakistan where he attended National University of Sciences and Technology (NUST) for his Bachelors. In 2019, he moved to Knoxville to pursue his further education at the University of Tennessee. During his PhD, Talha decided to obtain a concurrent Masters in Electrical Engineering from the university as well. Primarily, he is employed as a graduate research assistant with emphasis on model reduction techniques for non-linear dynamical systems for his PhD. Talha graduated with his Master of Science in May 2023 and is now focusing on completing research work for his PhD at the University of Tennessee.